III. Dosimetry

As we have already shown in the introduction, the low energy photons studied in this work are very easily attenuated in matter, especially in high Z materials, like the encapsulation of the seeds. Consequently, a whole new characterisation of the dosimetric function is mandatory for each new type of source prior to its use in clinics. The first part of this study will contain the determination of this basic data for sources of ^{103}Pd and ^{125}I recently commercialised, using measurements and Monte Carlo calculations. This basic study has permitted to look in detail into some of the problems that may occur during this type of study and that may influence the parameters for clinical use. We will try to assess which steps of this determination can induce such inaccuracies in the clinical data and how to minimise their effects.

A. Material

The measurements around low energy photon brachytherapy sources are quite complex due to, amongst others reasons, the very low dose rates and the very high dose gradients involved. This implies the use of high-spatial resolution detectors that have also a very high sensitivity. The choice of detectors is consequently very limited. Traditionally, TLDs are used because of their sensitivity, their relatively good tissue equivalence, their good linearity in the low dose range and the possibility to obtain them in very small sizes, which allows a quite high spatial resolution.

Other detectors have been considered in this work, like diamond detectors or diodes. They also have very small dimensions but their sensitivity is too low for the sources we were using. Our sources are intended for use in prostate implants, in which high activities are not required. The maximum activity that IBt could offer us without modifying the production technique was of about 2 U for ^{125}I and 2.5 U for ^{103}Pd. The dose rates obtained with these seeds were comprised between ~2.5 cGyh^{-1} for the most active seeds at 1cm and ~0.010 cGyh^{-1} for the less active seeds we have used and at the largest distance where we have measured (5 cm for ^{103}Pd and 7 cm for ^{125}I). It was not enough to reach a sufficiently high signal/noise ratio with diamond detectors or diodes farther than about 1 cm.

Films were also considered, but the dynamic range and the non-linearity of the classic silver halide films X-omat V were very limiting due to the very high dose gradients involved. The dose after 24 hours of exposure for a typical Pd seed varies from 240 cGy at 0.5 cm to 60 cGy at 1 cm and to 0.3 cGy at 5 cm. So their range of linearity limited to doses between 5 cGy and 100 cGy limits the use of silver halide films to a very small portion of space at a time. Even the extended range of the new films from Kodak EDR2

from 25 cGy to 400 cGy is not sufficient. This problem could have been solved with film with an even larger range like gafchromic films, but they are not sensitive enough for our purpose. The smaller possible dose for the classic MD55 is around 8 Gy. This was not reachable in a manageable time at a distance from the seed. Quite recently, a new type of Gafchromic film (RT) has been commercialised that is optimised for low energy photons. The dynamic range from 20 cGy to 2000 cGy could allow measuring the radial function from 0.5 cm to 5 cm in only two exposures. These films could be a very interesting detector for brachytherapy measurements. It should certainly be investigated in the near future.

Except for diodes, the results of any of these measurements techniques are the dose distributions around the seeds in solid medium. However, the data required for clinical use are the dose distribution in water, which is considered as the best tissue substitute in medical physics. It is consequently mandatory to obtain these dose distributions in liquid water with the use of Monte Carlo calculations. As was explained in the general introduction, many codes are available which can be quite different from each other. We have chosen to use two of these codes to calculate the dosimetric data of the new brachytherapy seeds of IBt. The first reason for using two codes was as a self verification. Later the use of the two codes has revealed itself to be much more interesting that just a verification of the method. We were led to analyse in more details the basic data used in these code and the comparison of the calculations became an endpoint in itself. In order to facilitate the understanding of this comparison, which is detailed in chapter III.C., we will first briefly describe in this chapter those two codes and their respective underlying philosophies.

1. Monte Carlo simulation

Monte Carlo (MC) simulation of particle transport processes is one of the main tools used in this study. These calculations are a faithful simulation of physical reality. The particles are first created in the source, following the description of the source geometry and emitter. They are transported in the medium on a certain distance. During that transport, interactions occur with probabilities given by the total cross sections. During these interactions, the particle is absorbed or scattered. New particles can eventually be created. The direction and energy of these scattered or produced secondary particles are determined according to the differential cross sections and they can be followed at their turn if needed. The procedure is continued until the particles are absorbed or leave the geometry (see Figure 16). Quantities of interest like deposited energy, particle fluence,… can be calculated by averaging over a large set of MC particle "histories". These quantities are subject to statistical uncertainty related to the number of simulated histories, N, that has been used during the simulation, usually decreasing usually with $N^{-1/2}$.

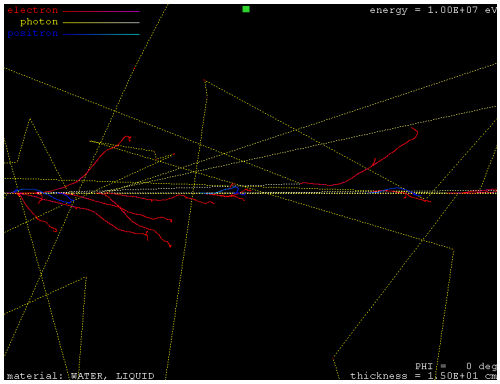

Figure 16: Example of the MC simulated transport of 50 photons (yellow) with an energy of 15 MeV in a slab of 15 cm of liquid water. Red lines are electrons and blue lines are positrons.

The idea of using random sampling, the basis of Monte Carlo calculations, to solve complex mathematical problems and build-up effects is not new. The first known documented attempt is the one of Compte de Buffon in his paper, *Sur le jeu de franc-carreau*, published in 1777 (Buffon 1777). This problem is known as "the problem of Buffon's needles". A century later, some people as Laplace (1886) or Lord Kelvin used random sampling to evaluate the value of π or to solve some time-dependent integrals. Lord Rayleigh (1899) even delved into this field near the turn of the century. Later, Fermi seems to have used statistical sampling to derive some of his famous "guesses" (Briesmeister 2000).

But the real start of Monte Carlo techniques is related to the first atomic bomb and to the emergence of computers during the Second World War. Credit for inventing the Monte Carlo method often goes to Stanislaw Ulam (Ulam and Metropolis 1949, Ulam et al. 1947), a Polish born mathematician who worked for John von Neumann on the United States' Manhattan Project during World War II. Ulam is primarily known for designing the hydrogen bomb with Edward Teller in 1951. He invented the Monte Carlo method in 1946 while pondering the probabilities of winning a card game of solitaire. Quoted in Eckhardt (Eckhardt 1987), Ulam describes the incident as:

> The first thoughts and attempts I made to practice [the Monte Carlo Method] were suggested by a question which occurred to me in 1946 as I was convalescing from an illness and playing solitaires. The question was what are the chances that a Canfield solitaire laid out with 52 cards will come out successfully? After spending a lot of time trying to estimate them by pure combinatorial calculations, I wondered whether a more practical method than "abstract thinking" might not be to lay it out say one hundred times and simply observe and count the number of successful plays. This was already possible to envisage with the beginning of the new era of fast computers, and I immediately thought of problems of neutron diffusion and other questions of mathematical physics, and more generally how to change processes described by certain differential equations into an equivalent form interpretable as a succession of random operations. Later … [in

1946, I] described the idea to John von Neumann, and we began to plan actual calculations.

The construction of the first computer, ENIAC (Electronic Numerical Integrator and Computer) for Aberdeen at the University of Pennsylvania had given the idea to John Von Neumann to use it for thermonuclear weapon calculations. The first computerized MC simulations have been performed just after the War, in 1947, to solve neutron diffusion and multiplication problems in fission devices. After that, the technique has immediately found multiple applications. Already in 1948, it had been successfully used to describe cosmic ray showers and to solve partial differential equations.

The fast development of computer programming language and calculation power has permitted to write more and more sophisticated codes and even to write in the 1960s a general-purpose code, i.e. a code that was no more linked to one specific problem.

The two codes used in this work are descendant of those general-purpose codes. The appearance of MC techniques in the field of Medical Physics took place in the 1970s and early 1980s. Due mainly to the slowness of the computers of that period, only very simple geometries could be modelled like point sources in homogeneous phantoms. But it was already a very good alternative to measurements for example to derive photon spectra from radioactive sources (Verhaegen and Seuntjens 2003).

To perform a MC simulation, the physics basics needs to be interpreted in the form of algorithms that allow performing the transport calculations in a realistic time. To reach this aim, approximations are unavoidable. Basic data are also required, such as the total cross section values, and the differential cross section data. The following paragraph give a presentation of the way the two codes we have chosen, MCNP4C and EGSnrc, perform the simulations.

a) Photon transport

(1) MCNP4C (Briesmeister 2000)

MCNP4B/C is a general-purpose code that can be used for coupled neutron/photon/electron transport. The code treats an arbitrary three-dimensional configuration of user-defined materials in geometric cells bounded by first- and second-degree surfaces and fourth-degree elliptical tori. The cells are defined by the intersections, unions and complements of the regions bound by surfaces that are defined by supplying coefficients to the analytic surface equations or known points on the surfaces.

The user must supply an input file describing the source and of the geometry of the problem. It contains also the choice of physical treatment, detailed physics or simple physics, and the value of a number of other

parameters governing the transport. Finally, it must contain the kind of output (tally) desired by the user.

So, in this code, two kinds of treatments are possible for photons: the "simple physics" and the "detailed physics". These treatments differ by the amount of approximations involved and by the CPU time needed for the calculations. The "simple physics" is sometimes sufficient, when the transported particles are of high energy for example, and permits to save calculation time.

(a) Simple physics

This treatment is intended for high-energy photons. In this case, different simplifications can be applied. For the photoelectric effect, the energy of the ejected electron is the energy of the incoming photon, without creation of fluorescence photons. The Compton effect is assumed to occur on free electrons at rest, so the Klein-Nishina (K-N) equation is used to calculate the differential cross section. Finally, the Rayleigh interaction is ignored.

In this approximation, the angular distribution of a photon scattered at an angle q with respect to the incident direction is predicted by the Klein-Nishina formula by the differential scattering cross section ds/dW:

$$\frac{ds}{d\Omega} = Zr_0^2 \left(\frac{1}{1+a(1-\cos q)} \right)^2 \left(\frac{1+\cos^2 q}{2} \right) \left(1 + \frac{a^2(1-\cos q)^2}{(1+\cos^2 q)[1+a(1-\cos q)]} \right) \quad \textbf{(35)}$$

where $a \equiv E_g / m_0 c^2$ and r_0 is the classical electron radius (2.817938×10^{-13} cm).

(b) Detailed physics

This treatment includes coherent scattering and accounts for fluorescence photons and Auger electron emissions after photoelectron absorption. The electron binding effect is also taken into account.

For Compton scattering, the angle of scattering, the new energy of the photon and the recoil kinetic energy of the electron are determined from sampling of the differential cross sections. The recoil kinetic energy can be deposited locally, or transported according to two different modes: one where the electron is actually transported as a new particle, or one where a thick-target bremsstrahlung model (TTB) is used. This model generates electrons, but assumes that they travel in the direction of the incident photon and that they are immediately annihilated. Any bremsstrahlung photons produced by the nontransported electrons are then banked for later transport. Incoherent scattering is assumed to have the differential cross section: $s_I(Z,a,m)dm = I(Zn)K(a,m)dm$, where $I(Z,m)$ is an appropriate

scattering factor modifying the Klein-Nishina equation $K(a, m)$ to take into account the binding effect.

For coherent scattering, only the deviation angle must be computed and the transport of the photon continues. The differential cross section is given by: $s_2(Z,a,m)dm = C^2(Z,n)T(m)dm$, where $T(m)$ is the energy-independent Thomson cross section: $T(m) = pr_0^2(1+m^2)dm$, and $C(Z,n)$ is again a form factor taking into account the binding effect with $u = \sin(q/2)/l$ and $m = \cos(q)$.

The photoelectric effect consists in the absorption of the incident photon of energy E_g, with the consequent emission of several fluorescent photons or Auger electrons and the ejection (or excitation) of an orbital electron of binding energy $e<E_g$, giving the electron a kinetic energy of $(E_g - e)$. In the MC simulation, as for the treatment of the Compton scattering, the emitted electrons can be followed completely as new particle or in the TTB approximation, or be deposited locally according to the user's choice. The fluorescence photons are assumed to be emitted isotropically and are transported, provided that their energies are higher than the photon cutoff energy chosen by the user.

The pair production is only considered in the field of a nucleus with the threshold of $2m_0c^2[1+(m_0/M)] @ 1.022MeV$, where m_0 is the mass of the electron and M the nuclear mass. The created particles are transported or not depending to the user's choice.

(2) EGSnrc (Kawrakow and Rogers 2003)

The EGSnrc code consists in two subroutines, HATCH and SHOWER, written in MORTAN. They in turn call other subroutines, some of which call three user-written subroutines called HOWFAR, HOWNEAR and AUSGAB (see Figure 17). To use EGSnrc, the user has to write a "user code" consisting of a MAIN program, the two subroutines that describe the geometry of the problem, HOWFAR and HOWNEAR and one subroutine describing the output (scoring), AUSGAB. Usually, MAIN will perform the initialisations needed for the geometry subroutines and set the values of certain EGS COMMON variables as the names of the media used, the cutoff energies, … MAIN then calls the HATCH subroutine that does some initialisations and extract the material data for the media from a data set called PEGS. This data set must be created previously. After that step, MAIN calls SHOWER. Each call to SHOWER results in the generation of one particle history. The arguments of SHOWER specify the parameters of the incident particle initiating the cascade. A certain number of flags are available that permit to the user to switch on or off some refinement in the calculations as relaxation, bound Compton, etc… in order to adapt the level of approximation to the case the user is treating.

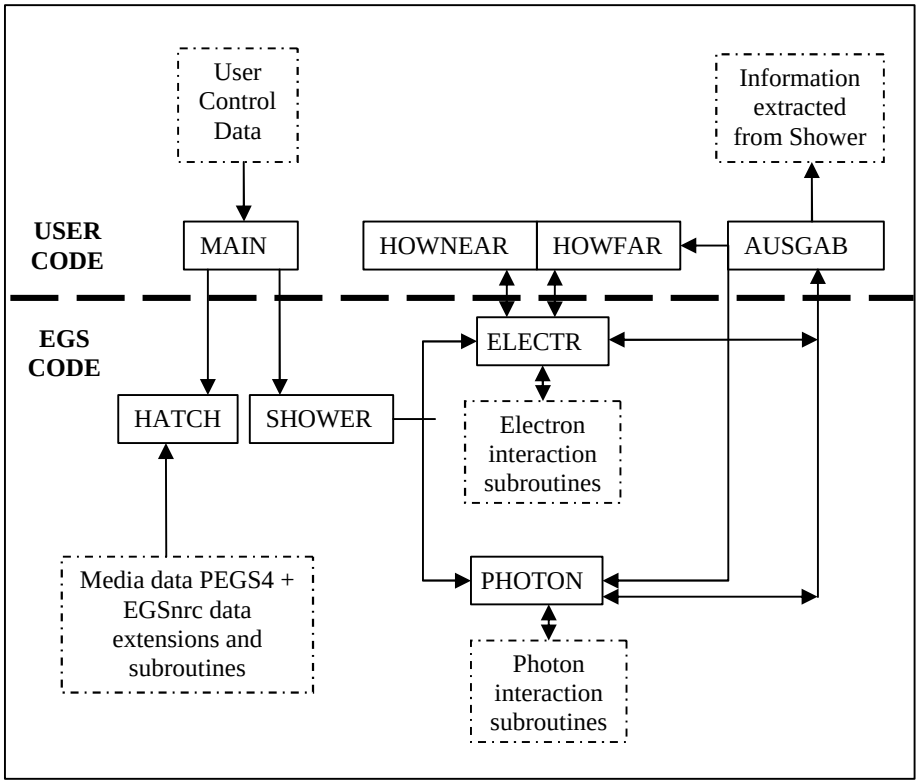

Figure 17: Simplified structure of the EGSnrc code when used with a user-code.

(a) Compton Effect

For the Compton interaction, EGSnrc includes the Doppler broadening effect and the binding effect. The cross section sets in PEGS are however created using the Klein-Nishina equation. The inclusion of Doppler broadening and binding effects is performed by rejecting a number of interactions with the probability $(1-\sigma_{compt}^{tot}/\sigma_{KN}^{tot})$, where σ_{compt}^{tot} is the total cross section including the corrections and σ_{KN}^{tot} is the total cross section in the K-N approximation. This permits to include or not these features without the need to create a new set of PEGS data. As shown in Figure 18 for an initial photon with energy less than 35 keV, bound Compton has quite an important effect on the cross sections and can not be neglected.

The vacancy created by the Compton interaction is known. The relaxation of shell vacancies with binding energies above the specified transport threshold energies is performed using the subroutine RELAX and may lead to the creation of fluorescence photons and Auger and Coster-Kronig electrons. The remaining excitation energy below the threshold is deposited.

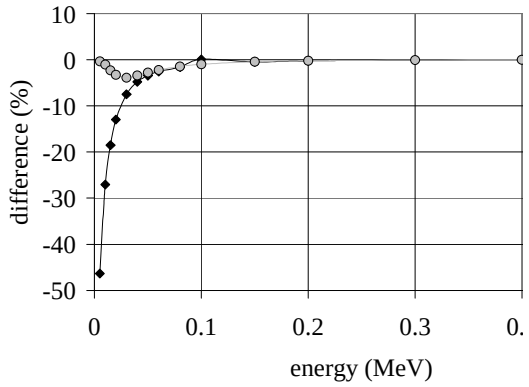

Figure 18: Differences between the cross section calculated for water with the Klein-Nishina equation and the cross section taking into account the binding effect and Doppler broadening. The circles are the differences on the total cross sections and the diamonds are the difference for Compton cross sections. (calculated with EGSnrc).

(b) Photoelectric effect

In EGSnrc, a detailed simulation of the photoelectric effect is the default case. It is however possible, using a flag, to switch off this detailed modelising. In the detailed simulation, the photon of energy E_γ is absorbed by an atom and a photoelectron is emitted. The cross sections for this effect are those tabulated by Storm and Israel (Storm and Israel 1970). The atom is let in an excited state and the relaxation process is treated as for Compton effect by the subroutine RELAX. For compounds and mixture material, this detailed simulation does not use an effective atomic number to determine the probability of interaction, but uses the real stoichiometric index to determine the atomic number of the element the photon is interacting with. When the interacting element is determined, the number of the shell with which the interaction takes place is sampled. The photoelectron can be emitted with the energy $E_g - E_b(Z)$, where $E_b(Z)$ is its binding energy. The energy left to the atom is then dissipated using the subroutine RELAX.

If the detailed simulation is not required, a photoelectron with an energy E_γ is simply created and no relaxation is considered.

To choose the direction of the photoelectron, two possibilities exist, controlled by the flag IPHTER. If the flag is set to zero, the photoelectron receives the direction of the initial photon. If the flag is set to 1, the direction is sampled from the Sauter angular distribution (Sauter 1931, Bielajew and Rogers 1986).

(c) Coherent scattering

The cross sections used for this effect are those of Storm and Israel (1970) with form factors of Hubbel and Øverbø (1979). The sampling for the Rayleigh production is accomplished only if the flag IRAYL is set to 1. Moreover, the data including Rayleigh effect must have been calculated for the treated material in the PEGS files. Coherent scattering is mainly important for low energy simulation and can be omitted when high energy photons are transported.

b) Electron transport

Contrary to photons, it is generally unrealistic to try to model electron interactions with matter interaction per interaction; the number of interactions to consider becomes generally too large. Consequently in MC simulations, a technique called Condensed History (CH) has been developed based on multiple scattering theories. In this technique, the path of the electron is divided in steps. The length of these steps must be chosen small enough so that the energy loss is small compared to the electron kinetic energy, but large enough to include a large number of interactions to justify the use of multiple scattering theories. In this case, the global angular deflection and energy loss for many individual collisions can be sampled from probability distributions based on the multiple scattering theories.

There are two kinds of CH techniques: Class I and Class II. In a Class I algorithm, all the interactions are grouped. A predetermined set of pathlenghts is used and the sampling of interactions is performed at the end of the step. The best way to choose the step length is so that, on average, the energy loss must remain constant. In Class II algorithm, the catastrophic events, i.e. the events where the energy of particles set in motion (bremsstrahlung photons or electron set in motion by inelastic scattering) is above a certain threshold, are treated as individual interactions. The others, together with the elastic collisions, are grouped.

(1) MCNP4C (Briesmeister 2000)

MCNP4C uses a class I algorithm. The multiple scattering theories used in MCNP4C are the Goudsmit-Saunderson (Goudsmit and Saunderson 1940) theory for angular deflection, the Landau theory (Landau 1944) for energy-loss fluctuations and the Blunck-Leisegang (Blunck and Leisegang 1950) enhancement of the Landau theory. These theories are based on several approximations, but the main assumption is that the energy loss is small compared to the kinetic energy of the electron.

At the start of each major step, the collisional energy loss rate is sampled. In the absence of energy straggling, this will be a simple average value based on the collisional stopping power. In general, however, fluctuations in the energy loss rate will occur. The major steps are divided in *m* substeps. The number of substeps varies according to the energy of the electron or to the proximity of a boundary. Except for energy loss and straggling calculations, which are evaluated only at the beginning of the major steps, the detailed simulation of the electron history takes place in the sampling of substeps. The Goudsmit-Saunderson theory is used to sample the distribution of the angular deflections, so that the direction of the electron can change at the end of each substep. Based on the current energy loss rate and the substep length, the projected energy for the electron at the end of the substep is calculated. Finally, appropriate probability distributions

are sampled for the production of secondary particles. These include electron-induced fluorescent X-rays, "knock-on" electrons (from electron-impact ionization) and bremsstrahlung photons.

(2) EGSnrc (Kawrakow and Rogers 2003)

EGSnrc, like MCNP, uses a CH technique. Many track segments of the real electron random walk are grouped into a single "step". The cumulative effect of elastic and inelastic collisions during the step are taken into account by sampling energy and direction changes from appropriate multiple scattering distributions at the end of the step.

However, the CH scheme used in EGSnrc is a Class II algorithm for the simulation of electron transport. That is to say, bremsstrahlung processes that result in the creation of photons above an energy threshold k_c, and inelastic collisions that set in motion atomic electrons with kinetic energies above T_c, are both explicitly simulated and the secondaries transported. Such interactions are also referred to as "catastrophic" collisions. Sub-threshold inelastic and radiative events and elastic collisions are subject to grouping. CSDA, the Continuous Slowing Down Approximation, assuming that particles lose energy in a continuous way and at a rate equal to the stopping power, is used to describe the sub-threshold energy loss processes. The multiple elastic scattering theory used in EGS4 was an approximation for small angles known as the Molière theory. This has been modified in EGSnrc where an exact formulation is now used.

In practical situations one has to deal with interfaces between different materials. If an electron is close to an interface between two materials, portions of its curved path may be in different material and so the trajectory is different than the simulated one. In the original EGS4 version, this problem associated with the condensed history simulation of electron transport, which has become known as the interface artifact (Bielajew et al. 1985), was entirely ignored. To address the interface artifact, a refined boundary crossing algorithm (BCA) was incorporated in the subroutine PRESTA. According to this algorithm, the electron is not allowed to take a step longer than $t_\wedge$, $t_\wedge$ being the perpendicular distance to the closest boundary, unless $t_\wedge$ becomes smaller than t_{min}, a user defined minimum step-length for boundary crossing. For $t_\wedge < t_{min}$, lateral deflections are switched off and the particle is transported, as in the case of standard EGS4, on a straight line to the boundary.

Foote and Smyth (1995) have demonstrated that the approach of forcing a multiple scattering event at the boundary causes a singularity in the simulated particle fluence. The singularity results from the fact that there is a non-zero probability for scattering parallel to the boundary. To overcome this problem an exact boundary crossing algorithm has been implemented into EGSnrc, i.e. the simulation goes over into a single elastic scattering mode whenever an electron comes closer than t_{min} to a boundary. Whereas in

the case of PRESTA, one of the criteria to determine t_{min} was to assure the applicability of Molière's MS theory, in EGSnrc the only criterion for t_{min} is efficiency (because of the multiple scattering theory employed which is applicable for all step-sizes).

c) Comparison of the two codes

These two codes have been made initially for very different purposes. MCNP, which stands for Monte Carlo N-Particles, and its precursors, were developed at Los Alamos to treat problems related to nuclear reactors. It was in its first version, called MCN, dedicated to neutron transport. In 1973, it has been merged with MCG, a Monte Carlo code that treated high-energy photons to form MCNG, and then to MCP to accurately model neutron-photon interactions with a detailed treatment of photon transport down to 1 keV. Electron transport was only added in MCNP4A released in 1990.

In contrast, EGSnrc is descendant of a code called SHOWER written in its initial form for high-energy electrons incident on lead targets of a cylindrical geometry. This code and its successors were dedicated to be used by experimental physicists working with linear accelerators. It was used amongst others at the Stanford Linear Accelerator Centre (SLAC) in the 1960s where codes capable of simulating electromagnetic cascade showers in the counters were needed. (Bielajew et al. 1994)

As the main goals of these codes were initially so different, their philosophies are equally different. MCNP4C is a very user-friendly code. It only needs from the user an input file describing the problem. The tools to describe the geometry are very efficient and practical. It is extremely easy to describe very complex geometries like, for instance, the geometries of nuclear reactor cores. EGSnrc is much less user-friendly to describe the geometries. Some build-in user codes exist for special geometries (cylinders for example) that can certainly help. There is even since the beginning of 2004 a new very easy GUI interface for these build-in codes, called EGSnrcMP, very similar to the EGSnrc/beam interface. However, when a general geometry is needed, the user must go through real programming in the language developed for EGS called MORTRAN. On the other hand, this gives some more freedom than with MCNP to analyse physics in a more detailed way.

Even if the first versions of these codes did not use similar approximations for the physics, or even did not implement the same physical phenomena, they have converged with the years and the successive improvements toward a quite similar treatment of photon interactions. In the latest versions, the details of the photon interactions are the same with the use of bound Compton scattering, the treatment of the atomic relaxation problem after an interaction and the possibility to account for coherent scattering. For electrons, the methods are still fundamentally different as one

code is a Class I code and the other is a Class II. Another divergence in algorithm could concern the boundary-crossing algorithm. It has been improved recently in EGSnrc with the use of single elastic scattering mode for the transport through a boundary, which makes a difference for dose at interfaces. However, as in the problem of low energy photons the electrons plays a very limited role, we have not in this work analysed the eventual agreement of the two codes for electrons, only photon transportation has been compared.

Cross section data remain different between the two codes in their present versions, even for photons. MCNP uses cross section data and form factors for coherent and incoherent photon scattering from Storm and Israel of 1967 or from ENDF (Hubbell et al. 1975), the fluorescence data are taken from Everett and Cashwell, report LA-5240-MS (Everett and Cashwell 1973) (DLC200). The photoelectric data present a difference of about 10% with the data published by NIST (Hubbell and Seltzer 1995) in the region of 20 keV – 30 keV (see Figure 19). This library has then been updated by T. Bohm et al. (2003) to correct the photoelectric cross sections. They used data from EPDL (Cullen et al. 1997) for photoelectric effect between 1 and 50 keV. This new library was tested in this work.

In EGSnrc the cross section data for photoelectric effect are from Storm and Israel (1970). The cross section data, even if they were closer to the NIST data than for MCNP, were not optimal, so an updated library, compiled at McGill Institute by Hobeila and Seuntjens (2002) has also been tested. The comparison of these two libraries with the NIST data is shown on Figure 19.

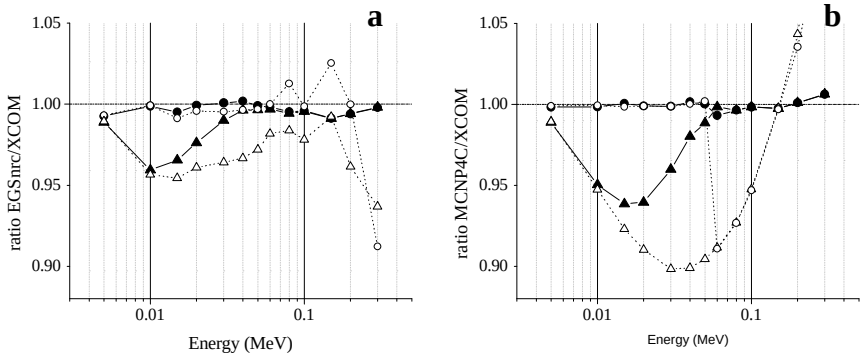

Figure 19: Comparison as a function of the photon energy of the attenuation in water calculated with EGSnrc (a) or MCNP4C (b) MC codes and the attenuation given by XCOM/NIST (Hubbell and Seltzer 1995). The triangles are the ratios between the original values of the codes and the XCOM/NIST coefficients and the circles are the ratios between the corrected cross section data and the XCOM/NIST coefficients. The full lines and filled symbols correspond to the total attenuation, the dotted lines with open symbols to the photoelectric effect.

2. Measurements

a) Thermoluminescent dosimeters

(1) Theoretical introduction: basic mechanism

Some inorganic crystals like Lithium Fluoride (LiF), Calcium Fluoride (CaF_2),… activated with Manganese, have the propriety to trap the electrons and holes produced by an incident ionising radiation within the bandgap of the crystal. They are called Thermoluminescent Dosimeters (TLDs). The electrons are elevated from the valence band to the conduction band but are captured in one of the trapping centres. If the energy difference between the trapping centres and the valence band is large enough, the probability that these electrons are freed by thermal excitation at ordinary room temperature is very low and they accumulate in the traps as long as the crystal is exposed to radiation. The holes are trapped in the same way in hole trap of energy slightly above the valence band. A sample of TLD material will then function as an integrating detector in which the number of trapped electrons and holes is a measure of the number of electron-hole pairs created by the radiation.

To know the number of trapped electrons and holes, the temperature of the TLD must be progressively raised. The composition of the TLD material, and especially the impurities it contains, determines the energy level of the traps and so the temperature at which the electrons can acquire enough energy to jump in the conduction band to be released. If this temperature is lower than the temperature needed to release the holes, the electrons can move to the trapped holes and recombine with them. The resulting energy liberation is emitted as a photon. The reverse process is also possible in which the holes are freed first and migrate to the trapped electrons. If the energy emitted is in the range of 3 to 4 eV, the emitted photons are in the visible spectrum, this is the basis of TLD signal. These photons are detected by a photomultiplier device in order to produce a measurable electrical signal. The light yield is recorded as a

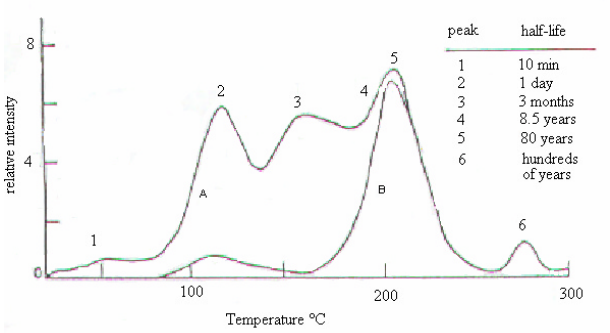

Figure 20: Glow curve for LiF:Mg:Ti (TLD 100) annealed for 1 h at 400°C followed by: A. cooling (10^3 °Cmin^{-1}) to normal ambient temperature; B, 16 h anneal at 80°C followed by irradiation. The approximate value of the half-life of each peak is also shown (Mason et al. 1976)

function of the temperature of the TLD in a *glow curve* (see Figure 20). The area under the glow curve is related to the number of photons emitted and thus to the radiation exposure. After the reading, the TLD sample can be heated to quite high temperature in order to deplete all the traps. It is then possible to use it again for another measurement.

(2) Dosimeter characteristics

There are different types of TLD materials, with different characteristics. The most commonly used are the lithium fluoride, LiF:Mg:Ti, called TLD-100, and $Li_2B_4O_7$:Mn because of their tissue equivalence. Others have been used for their sensitivity like $CaSO_4$:Dy, Al_2O_3:C and CaF_2:Mn. TLD-100 are the detectors that have been used in our measurements. In these TLD, the ratio $^{6}Li/^{nat}Li$ is 7%. The traps are created by the impurities and the defects in the crystal. This material shows a very low fading effect at room temperature and has a low effective atomic number (8.27). The later characteristic is the reason why the energy deposited in LiF is closely related to the dose in water or living tissue over a wide range of photon energies.

The TLDs were very interesting for our study because of their sensitivity and the linearity of their response function. This has been studied by Meigooni et al. (1995). They show that, if nitrogen is used during the reading, small TLDs of $1mm^3$ can be used without nonlinearity corrections for measurements down to 1 cGy with a dispersion of 5%, and to 15 cGy with a dispersion of 2%. This has been tested on the TLDs used for this study (see chap III.B.b.). For higher doses, this material shows a nonlinear increase of the response known as supralinearity.

Because of the predominance of the photoelectric effect for low-energy photons of ^{125}I and ^{103}Pd, it is possible that the dose at a point in a phantom could be affected by replacing part of the phantom with a LiF chip. In particular, there can be an interchip shielding effect when one chip is placed in the shadow of another and there can be an interchip scattering effect when chips are set very close to each other. Those effects have been studied by Meigooni et al. (1995). The geometry chosen for our phantom takes their results into account to reduce these effects.

(3) Energy correction factor.

The TLD used for the measurements, as many other detectors, are unfortunately not constant in response with energy (see Figure 21). A correction factor must be used for the measurement of absolute doses.

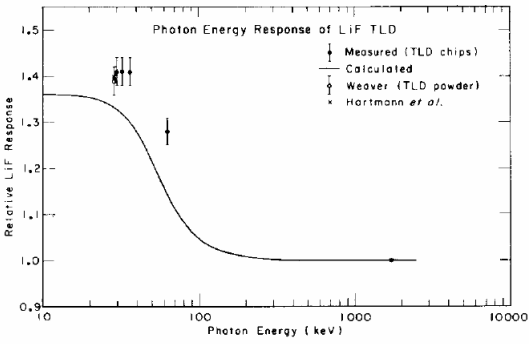

Figure 21: Response of LiF TLD per unit dose to water for different energy X-rays. These data points are normalised to 4-MV X-rays. The photon energy represents monoenergetic equivalent for the X-ray spectra. The solid curve is the ratio between the mass energy absorption coefficient of LiF and that of air. (Figure taken from Meigooni et al. 1988)

There are few sources available in the literature. Two of these studies that have been used in this work are described below:

- The first source is a series of papers from Weaver et al. (1984, 1999). Weaver's method is the following: TLDs were first irradiated in a ^{60}Co beam to obtain the calibration factor for ^{60}Co, $C(^{60}Co)$. The calibration factor for ^{125}I, $C(^{125}I)$ is then measured using a 5 cm-diameter ring of 12 small plastic tubes suspended in air from a low-mass stand. One or two ^{125}I seeds were placed in each tube and a thin-walled ion chamber, calibrated at a range of low energies, was placed at the centre of the ring of seeds (see Figure 22). With the ion chamber, the exposure rate in free air at the centre of the seed ring was measured and converted into dose-to-water using the R-to-cGy conversion factor. The ion chamber was then replaced by a series of TLD capsules, which were irradiated for a known time. A correction was applied to take into account self-attenuation in the medium of measurement.

The ratio $P = C_{cal}(^{60}Co)/C_{ca}(^{125}I)$ is 1.39 (Weaver 1984) and 1.42 (Weaver et al. 1989) for model 6702 and 1.47 (Weaver et al. 1989) for model 6711. Taking into account the uncertainty of about 5% in the calibration of the seeds, the authors assume that these values are not significantly different.

- A second method to measure this energy correction factor is described by Meigooni et al. (Meigooni et al. 1988). Their method is quite different. 100 TLD chips were first calibrated in a 4 MV X-ray beam. The dose response curve was then obtained for 60, 80, 100 and 250 kV X-ray beams. For these photon energies, the chips were irradiated in air to exposures simultaneously measured using a National Bureau of Standards (NBS) calibrated Spokas chamber. The charge collected by the chamber was

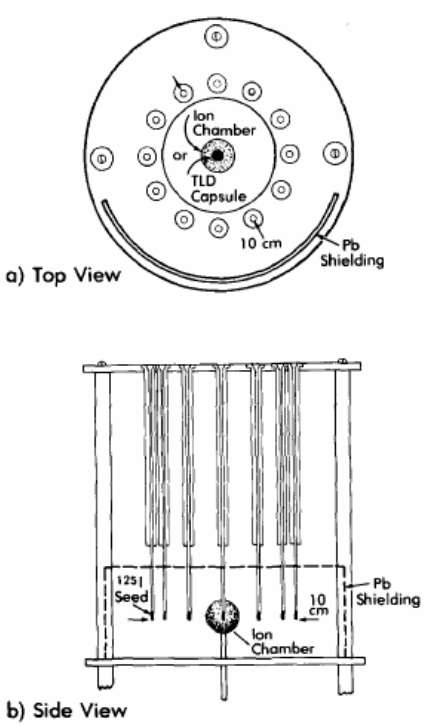

Figure 22: Stand used for irradiation of TLD capsules by an ^{125}I array. After the exposure rate was measured by an ion chamber, the latter was replaced by a TLD capsule supported by a rod similar to the ion chamber stem (Weaver 1984)

converted to dose to a small mass of water in air by multiplying by the chamber's exposure calibration factor, the exposure-to-dose conversion factor and the temperature-pressure correction factor. The aluminium HVL of each spectrum was determined in the conventional way under narrow beam geometry thus allowing the LiF response to be related to the monoenergetic equivalent of each beam, which is 30, 32.5, 36.5 and 64 keV. In this way, the response of the chips to ^{125}I energies relative to 4 MV X-radiation was determined. The energy correction factor they found for ^{125}I is 1.41 ± 3%.

These two studies reach a very good agreement regarding the value of the energy correction factor for ^{125}I. We have therefore decided to use the value 1.40 ± 5% it in this work. The Figure 21 is interesting as it shows that the energy correction factor reaches a plateau below 30 keV. This allowed us to use the same energy correction factor for ^{103}Pd.

Although there is a whole paragraph about the matter in the updated recommendations of the AAPM (Rivard et al. 2004), this problem of the energy correction factor is not clear yet. Many questions are still opened and would need a dedicated study. It is still recognised as being the major source of Type B uncertainties for absolute TLD measurements in the low energy photon range, with a usually assigned value of 5% (Meigooni et al. 2000). Contrary to the way we are treating the corrections for TLD measurements in this work, the new TG-43 uses a single function of distance, E(r), grouping the energy correction factor and all the other effects that can influence the dose measured by the TLDs: volume averaging (influence of dose gradient in the TLD volume), detector self-absorption, medium displacement and conversion from measurement medium to liquid. They however do not recommend any value for that function. In this work, we have preferred to divide this into three separate effects: the energy response effect, the effect of the conversion from solid medium to liquid that we call

water equivalence effect and the effect due to the presence of the detector that we call TLD perturbation.

b) Phantom material

(1) Tissue or water equivalence: Basic concepts

Any material used to simulate a particular human tissue with respect to a set of physical characteristics is called a *tissue substitute*. For a material to be acceptable as a tissue substitute for photon and electron interactions the radiation absorption and scattering obtained with a given thickness or mass of material must be the same as that experienced in a similar thickness or mass of tissue (White 1978). A practical way to compare the radiation characteristics of materials is to compare the mass attenuation and energy absorption coefficients (μ/ρ, μ_{en}/ρ) and electron mass stopping and mass scattering powers ($S/\rho, T/\rho$) for a representative range of energies together with a typical, or average, density. There is no single chemical compound that matches the atomic composition of human tissue. Often, mixtures are employed in which the principal ingredient is a material that approximates tissue with respect to one or more radiation interactions. Other substances are added to rectify, as far as possible, the deficiencies of the base material. Hence, tissue substitutes are often mixtures of chemical compounds formulated so that their radiation interaction properties, rather than their atomic composition, match those of the body tissue to the degree necessary for the specific application over the desired range of radiation energies. Such materials have been engineered to match a variety of specific tissues, like lung, fat tissues, …. The same principle has been used to create *water substitute*. The advantage in this case is to obtain a solid material that can be used instead of liquid water when the experimental setup requires it.

The human body is composed essentially of water, so the usual material used to match the mean tissue in human body is water. Unfortunately, the very high gradients around low energy photon sources make it difficult to reach the required precision on the positioning of the detectors in water. We have already mentioned the difficulty to find another detector than TLDs that could be used easily in water, due to the very low

	WT1	RW1	PMMA	Water
H	8.1	13.2	8	11.2
C	67.2	79.4	60	-
N	2.4	-	-	-
O	19.9	3.8	32	88.8
Ca	2.3	2.7	-	-
Cl	0.1	-	-	-
Mg	-	0.9	-	-
density	1.015	0.97	1.19	1

Table 4: elemental compositions of the different materials in percentage by mass and density of the different phantom materials used in this work.

activity of the IBt seeds. We have therefore decided to use the TLDs in solid phantoms, which is the standard way to measure dose distributions around brachytherapy sources.

In order to minimise the corrections needed to convert measurements in solid medium into values in water, we have chosen to use a water equivalent solid medium. Materials like polystyrene, PMMA or solid water WT1 from RMI can be considered as good water equivalent materials for high energy photons. For low energy photons however, the photoelectric effect is more important, so materials that are good water equivalents for high energy photons but that contain, as WT1, high Z elements that have a very high cross section for photoelectric effect are not ideal for low energy photons. Other materials have become available which are made to match radiation characteristics of water for lower energies, one of them is RW1 from PTW Freiburg.

As a basis for the rest of the study, we have compared three of these materials, WT1, RW1 and PMMA to establish which one was the most relevant for our study. The composition and density of these materials, taken from ICRU 44 (1989) are listed in Table 4.

c) <u>Sources description</u>

The sources studied in this thesis are the InterSource-125 and InterSource-103 produced by the International Brachytherapy company, IBt, based in Seneffe, Belgium since 1996.

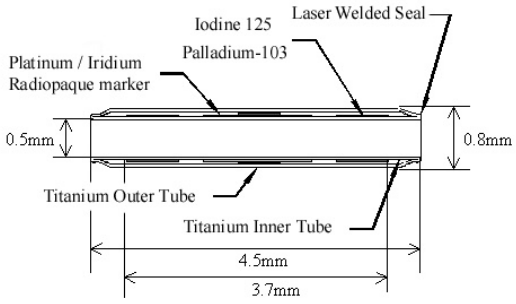

Figure 23: schema of the ^{125}I and ^{103}Pd InterSource seed geometry

The InterSource is composed of two concentric titanium tubes with a Platinum/Iridium alloy X-ray marker (90% platinum and 10% iridium). The radioactive iodine or palladium is deposited on the inner tube as three printed bands. The 3.7 mm active length of the source was determined by the outer edges of the printed bands (see Figure 23).

B. Method

1. Monte Carlo simulations

The method used for the simulations is explained in Chapter III.C. This section is intended to give a few more details about the modelisation that have not been dealt with in the publications.

a) Seed geometry

The geometry of the seed produced by IBt is shown on Figure 23. The geometry used for ^{103}Pd and ^{125}I is identical. It consists into two concentric titanium cylinders laser welded at the edges. In between is placed a Platinum/Iridium radio-opaque marker. The radioactive material is dissolved into a polymer matrix and is sprayed on the inner tube as three bands of painting. The external appearance of the seed is a hollow tube.

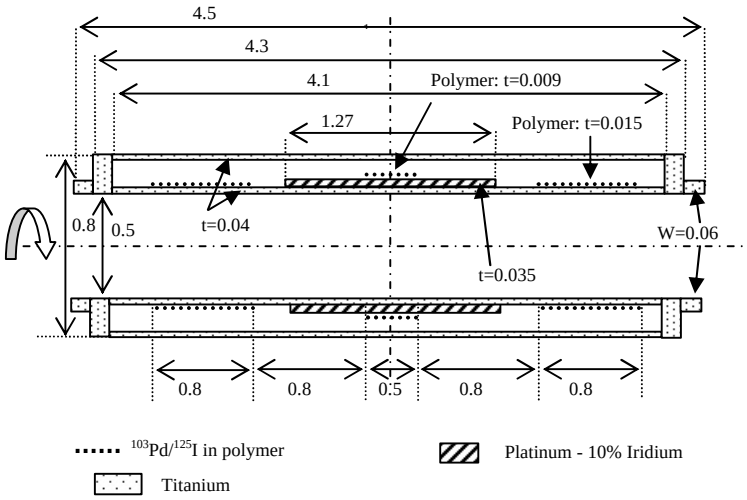

Figure 24: First model of the IBt seed in MCNP. The edges are modelled as cylinders.

Figure 24 shows the first geometry that was modelled in MCNP. It can be compared to the original geometry of the seed in Figure 23. All the dimensions are respected in the model. However, the real shape of the edges is unknown as it is a laser welded seal. It is also very likely that it varies slightly from one seed to the other. Consequently, we had to adjust the shape of the edges in order to obtain a good agreement with the measurements for the anisotropy function. As shown in Figure 25, we obtained already good results with this first model (called “cylinders” in Figure 25) except between 0° and 20°, which is on the longitudinal axis where it must be noted that the uncertainty is quite high for the measurements as well as for the calculations due to the high self-attenuation of the seed. However, to improve the results

on that axis, we have tried different other geometries of the weldings in order to simulate as well as possible the smooth shape of the real edges. The final design is the one described in Figure 26 where we have used two cones to model the smooth variation of the edges. The distance between the two cones and the thickness of the tips were adjusted in order to simulate the real welding.

Figure 25 shows as an example the variation of the anisotropy function at 2 cm for 3 different geometries of the edges, compared to the measurements. The difference between "thick edges" and "thin edges" is the distance between the two cylinders forming the tips of the seed (distance W on Figure 24). It is set to 0.08 mm for the thick model and 0.06 mm for the thin one. The influence of these edges is more important for ^{103}Pd; while for ^{125}I, the effect is small. A supplementary constraint is that the same geometry has to be used for both isotopes, as there are no differences in their method of fabrication. So, the model used for the rest of the study is the one called on the graphs "thick edges" as the improvement it brings for the Iodine seeds is more significant than the slight decrease in the agreement for Palladium. Indeed, the use of the thick edges model for ^{103}Pd decreases the agreement only on the longitudinal axis, where the uncertainty is very high while it remains very good for the other angles. The agreement that we have obtained with this model is very good, as can be observed in the "results" in ChapIII.C.

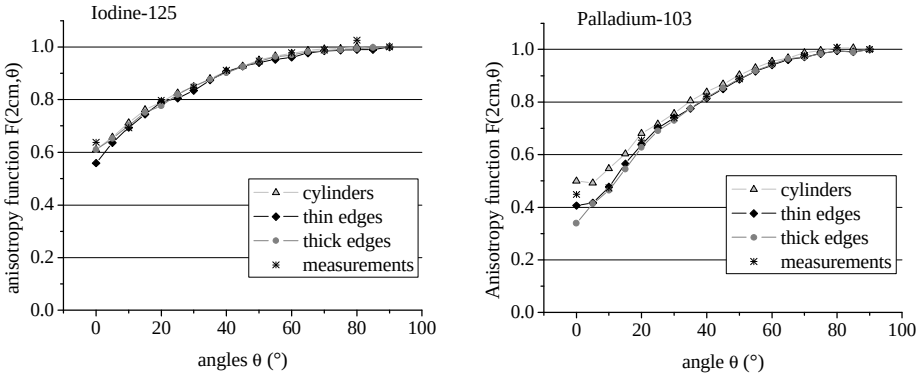

Figure 25: Example of anisotropy function calculated in solid water WT1 around a ^{103}Pd seed on the left and an ^{125}I seed on the right.

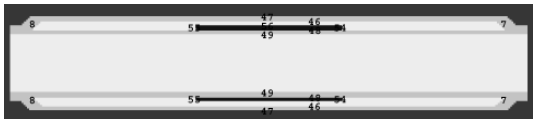

Figure 26: Schematic diagram of the seed as modelled in MCNP4C.

For EGSnrc some user codes are available like DOSRZ, FLURZ, … which only necessitate that the user write an input file, like in MCNP. However, we have preferred to write our own user code to keep more flexibility.

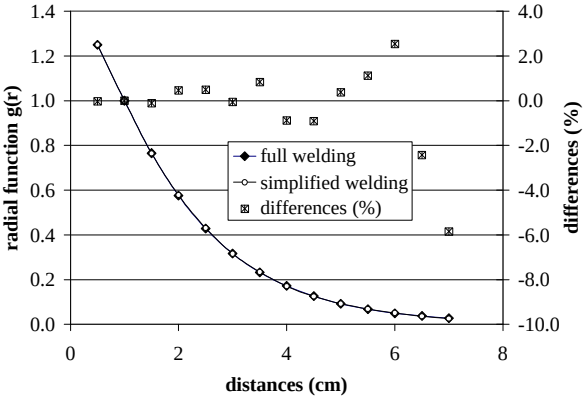

Figure 27: Comparison of the radial function for ^{103}Pd when the tips are modelled (full welding) or not (simplified welding).

Our goal was to calculate only the radial function in EGSnrc as a validation for the MC calculations, so in view of the higher complexity in the coding, the model of seed simulated with EGSnrc is somewhat simpler than with MCNP. The basic geometry is the same as described in Figure 24 except for the edges, where we have simplified the geometry by removing the tips of 0.6 mm thickness, which makes no differences on the transverse axis (see Figure 27 for ^{103}Pd seed). The geometry used in EGSnrc is shown in Figure 28.

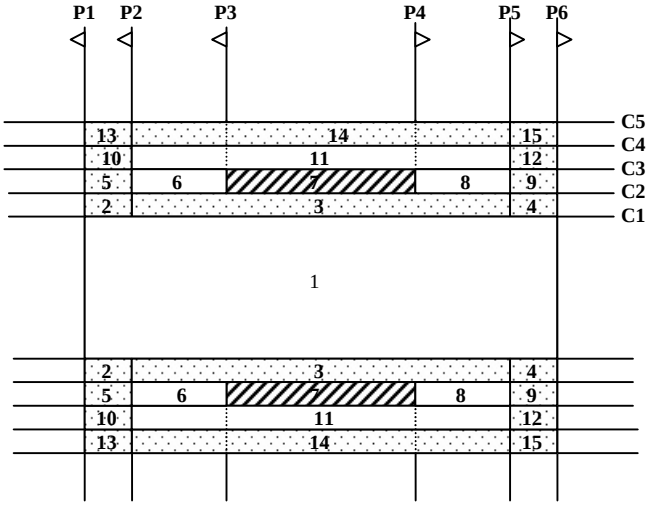

Figure 28: Schematic view of the model of InterSource used in EGSnrc. The numbers are the cells, Pi are the planes, with the direction of their normal indicated by the triangle and Ci are the cylinders. Different fillings are different materials: void areas are air, lined areas are platinum and dotted areas are titanium.

b) Scoring cells geometry

Two types of scoring cells have been used. The first one (Figure 29) has been used only for the MCNP calculations and allows to calculate in one run the anisotropy function and the radial function. The dose distribution around the seed is calculated using a mesh that consists in the intersection of cones centred at the centre of the seed with spheres also centred at the centre of the seed. The anisotropy function for one distance is calculated using the energy deposited in the cells comprised between two spheres in function of the angle and the radial function is calculated using the energy deposited in the cells comprised between cone 72 and 73 (see Figure 29) in function of the distance from the seed centre. The distance between the spheres determines the radial resolution and is 1 mm. The aperture of the cones determines the angular resolution of the anisotropy function, which is 5°.

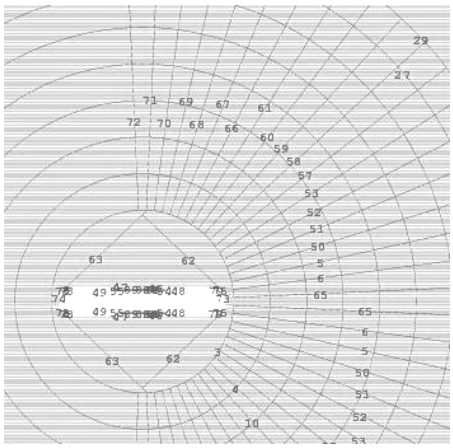

Figure 29: Schema of the scoring cells used to calculate the radial function in MCNP.

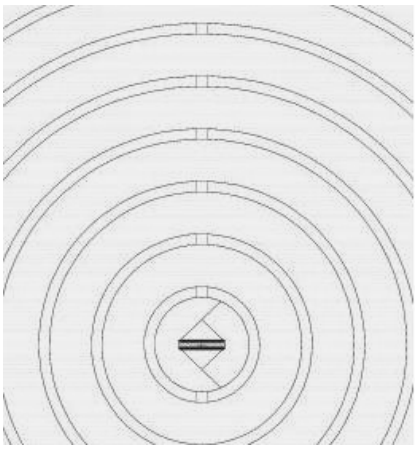

Figure 30: Schema of the scoring cells used to calculate the radial function in MCNP and EGSnrc.

This scoring geometry has been simplified for the comparison between MCNP and EGSnrc (Figure 30) as we where interested only in the radial function. The cells are defined by the intersection of spheres and planes. The distance between the spheres for the scoring cells is 1 mm and the distance between the two planes is also 1 mm.

c) Active layer definition

The position, energy and direction of each initial particle are sampled at the beginning of each history. From a MC point of view, the way the active layers are disposed inside the seeds implies that we should consider it as a multiple source problem. In this problem moreover, all the “sub-sources” do not have the same geometry, nor total activity as it is the

volumic activity of the solution which is constant and the amount of solution differs from one “sub-source” to the other.

The first information needed in order to sample the position of the emitted particles is the probability that a particle is emitted by part 1, 2 or 3 (see Figure 31). The theoretical volume of each layer can be calculated easily from Figure 31 and, as the volumic activity is constant for the three part of the source, it can be used to deduce the proportion of photons emitted by each layer. This gives a probability of 82.8% that the particle is emitted by zone 1 or 3 and 17.2% for zone 2. This ratio has of course an important influence on the initial part of the radial dose function and on the anisotropy, as can be seen on Figures 32 and 33.

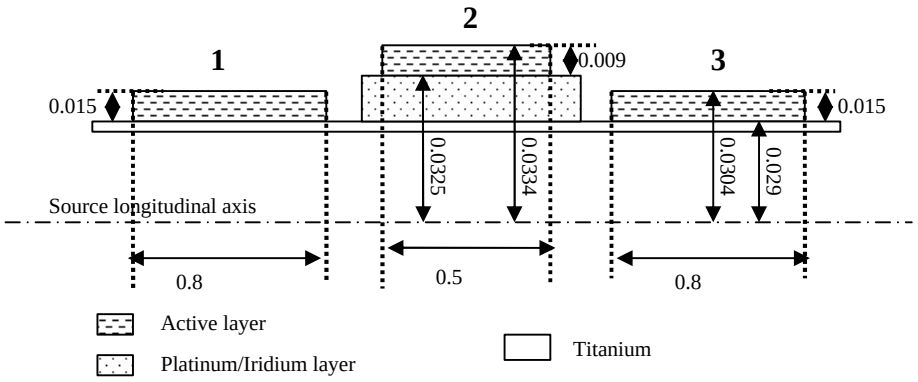

Figure 31: Idealised geometry of the active layers in the IBt seeds (distances in mm, not at scale).

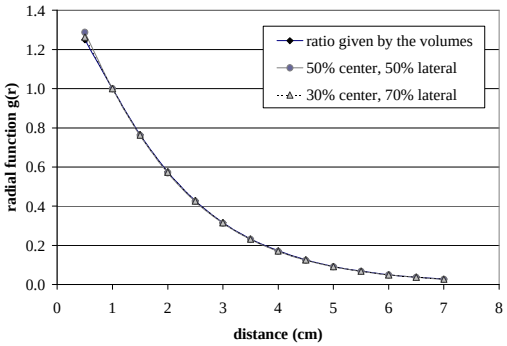

Figure 32: Examples of the modification of the radial function when the ratio between the activities of each radioactive layer is modified in the InterSource-103

There are several solutions in MCNP to model the position of multiple sources when they don’t have the same basic geometry. In this case, the radii used to describe them are different for the lateral sources and for the central one (see Figure 31).

The easiest approach is to divide the source into two different input files with the source definitions as shown next, one input file containing the lateral sources and the other containing the central source. In the first input file, the source particles are sampled between two cylinders of radius 0.0325 cm and 0.0334 cm. The radius from which the photon is emitted is first sampled, taking into account that the circumferences increase with the radius and that, consequently, it is more probable that a particle should be emitted from the outer radii. Then the longitudinal position is sampled between -0.025 cm and 0.025 cm, with an equal probability for each distance. The angular distribution is equally probable. In a second input file, the same radius sampling and angular sampling are utilised, this time, between 0.029 cm and 0.0304 cm and the longitudinal position is sampled between -0.185 cm and -0.105 cm and 0.105 cm and 0.185 cm with half of the probability for each side. The results of the calculations are then combined afterward using a weighting factor equal to the ratio of the "sub-sources" volumes. This is what has been used in general for the calculations performed with MCNP. The source definitions in the input files that describe that case are the followings:

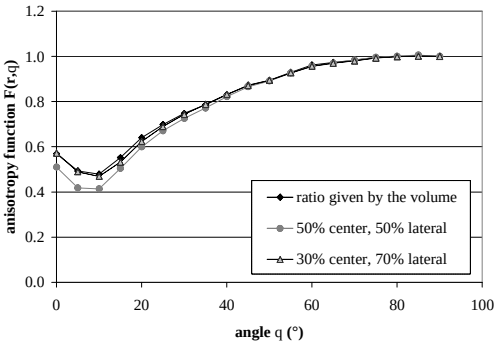

Figure 33: Examples of the modification of the anisotropy function when the ratio between the activities of each radioactive layer is modified in the InterSource-103

```
c source definition: input file 1 :Central source
c ************************************
SDEF POS=0 0 0 CEL=826 AXS=1 0 0 RAD=D2 EXT=D3  ERG=D1
PAR=2 WGT=1
SI1 L 0.00377 0.02720 0.02747 0.031 0.03546  $ iodine spectrum
SP1 D 0.15 0.398 0.742 0.258 0.0667
SI2 A 0.0325 0.0334
SP2 0 1
SI3 -0.025 0.025
SP3 0 1
```

```
c source definition: input file 2; Lateral source
c ************************************
SDEF POS=0 0 0 CEL=826 AXS=1 0 0 RAD=D2 EXT=D3  ERG=D1
PAR=2 WGT=1
SI1 L 0.00377 0.02720 0.02747 0.031 0.03546  $ iodine spectrum
SP1 D 0.15 0.398 0.742 0.258 0.0667
SI2 A 0.029 0.0304
SP2 0 1
SI3 -0.185 -0.105 0.105 0.185
SP3 0 0.5 0 0.5
```

However, it is also possible, even if not straightforward, to describe the entire sources in one input file using a definition at different levels and using dependent variables. The case of the IBt sources can be summarized as follow: three cylindrical sources with different extensions and radii. The first one is situated between -0.185 cm and -0.105 cm and its radius is between 0.029 cm and 0.0304 cm; the second one is situated between -0.025 cm and 0.025 cm with a radius between 0.0325 cm and 0.0334 and the third one is the symmetric of the first one. The source definition in the input file that describes that case is the following:

```
 184-      c source definition
 185-      c *****************
 186-      SDEF POS=0 0 0 CEL=D2 AXS=1 0 0 RAD FCEL D4 EXT FCEL
D3 ERG=D1 PAR=2 WGT=1
 189-      SI1 L 0.0201 0.0202 0.0227 0.0398 0.3575  $  Palladium energy
spectrum
 190-      SP1 D 0.2206 0.4193 0.1305 0.0007 0.0002
 191-      SI2 L 805 826 804                    level 1
 192-      SP2 D 0.414 0.172 0.414
 193-      DS3 S 5 6 7                          level 1
 194-      SI5 -0.185 -0.105                    level 2
 195-      SP5 0 1
 196-      SI6 -0.025 0.025
 197-      SP6 0 1
 198-      SI7 0.105 0.185
 199-      SP7 0 1
 200-      DS4 S 8 9 10                         level 1
 201-      SI8 A 0.029 0.0304                   level 2
 202-      SP8 0 1
 203-      SI9 A 0.0325 0.0334
 204-      SP9 0 1
 205-      SI10 A 0.029 0.0304
 206-      SP10 0 1
```

In this case, the number of the cell is the independent variable. Source 1 is located in the cell 805, source 2 in 826 and source 3 in 804. The classic MCNP SI/SP combination card samples the cell where the particle is emitted (line 191,192). The SI card gives the values taken by the variable and the SP card gives the related probabilities equal to the ratio between the volumes of the cells. Then, the value of the radius (RAD) and the extension (EXT) are dependent on the cell that has been chosen. That is indicated by the use of FCEL. Then the distributions for RAD and EXT are defined by the distributions D4 and D3.

The D3 distribution is described using a DS card to indicate that it is a dependent variable. The option used is S as it is followed by distribution numbers (other options are available). So, line 193 indicates that the radius must be sampled from distribution 5 when the particle is issued from cell 805, from distribution 6 when it is issued from cell 826 and from distribution 7 when the particle is issued from cell 804. The same principle is used for the extension of the sources in the DS4 card.

In EGSnrc, it is very natural to define even the three sources contained in the IBt seeds. The energy is sampled in the natural spectrum of ^{125}I or ^{103}Pd using a random number generated by the MORTRAN function $RANDOMSET. We have written the user code so that the user can choose the isotope at the beginning of the run or in an input file, so it is not necessary to recompile the entire program just to change the isotope.

Then, the position of the source is sampled, first by determining from which part of the source it is emitted, using the same volume ratio as for MCNP, then by determining the radial, longitudinal and angular position of the emission point within that part. The direction of emission is taken as isotropic, and the weight of the particle is 1.

d) Tally (output)

We have adopted two types of tallies in MCNP:

– the pulse height tally *F8, the asterisk meaning that the F8 tally is multiplied by the particle energy to give a result in MeV. This tally is equivalent to energy deposition in the scoring cell.

– the tally $F6 = W * T_l * s_T(E) * H(E) * r_a / m$ **(36)**

where W is the particle weight, T_l is the track length, E is the total particle energy, $s_T(E)$ is the microscopic total cross section at the energy E, $H(E)$ is a heating number defined for the photons in MCNP by: $H(E) = s_T(E)\sum_{i=1}^{3} p_i(E) \times (E - \overline{E}_{out})$ where $p_i(E)$ is the probability of interaction of type i (i.e. Compton scattering, pair production and photoelectric effect), $\overline{E}_{out}$ is the average exiting photon energy for

interaction *i*, r_a is the atom density (atoms/barns-cm) and *m* is the cell mass. This tally is a track length energy deposition tally. It gives the kerma in the cell. In the case of low energy photons, the electrons are not transported, as has already been mentioned, so kerma equals the absorbed dose. Consequently, the only practical difference between these two tallies is the statistical uncertainty. Indeed, as F6 is a track length estimator, no interactions are required to give a contribution to the result and consequently it is much easier to reach good statistics.

In EGSnrc, the scoring of the energy deposition and of the kerma in the cells of interest is performed in the subroutine AUSGAB. The argument of this subroutine is IARG. The value of that argument gives the kind of event that has just occurred or is about to occur. It can take up to 28 values. For example, the most commonly used IARG values are:

- 0: the particle is going to be transported by distance TVSTEP;
- 1: Particle is going to be discarded because its energy is below the energy cutoff;
- 3 particle is going to be discarded because the user requested it (geometry or variance reduction technique);
- 4: the difference between the energy of the incident particle and all of the final products is being deposited locally. This energy is due to sub-threshold relaxation events.

There are some less common values that have been extremely useful in our case for the calculation of the primary electron spectra in the microdosimetric part (see the Microdosimetry chapter) like:

- 18: return to PHOTON after a call to COMPT was made. So a Compton interaction has just occurred.
- 20: return to PHOTON after a call to PHOTO was made. So a photoelectric interaction has just occurred.

When an interaction occurs or after a step for electron transport, the quantity EDEP is automatically recorded. It is the energy deposited at each interaction or each step of a particle. To score the dose absorbed in the material of the cells, we have scored the energy deposited by each particle in each region of interest (IRL) and that for each batch (I) in a matrix called EDEPT(I, IRL). At the end of the computation, the values obtained for each batch are added to give the total energy deposited in each cell. The division into batches allows evaluating the statistical uncertainty for the computed value. A minimum of 10 batches was always used. We know the volume and the composition of each cell, so the absorbed dose can be simply calculated by dividing the deposited energy by the mass of the cell.

To calculate the kerma in each cell, we use the variable VSTEP that is automatically recorded and that gives the actual straight step length after truncation by the geometry. The kerma can be deduced by multiplying by the

energy absorption coefficient and the actual energy of the particle. The energy absorption coefficient are calculated on the fly for each particle step using functions that give μ_{en} as a function of the energy in the material contained in the cell. Those functions have been calculated using different polynomial fits for different energy regions on the values listed in the XCOM library (Hubbell and Seltzer 1995) or obtained from XmuDat (Nowotny 1998). This is a program freely distributed by the IAEA, which calculates the attenuation and energy absorption coefficients for any material between 1 keV and 50 MeV. This program offers the possibility of using the same library as the XCOM distribution. We have calculated those fitting functions to keep the difference between the fitted values and the original data below 0.1% for energies ranging between 5 keV and 500 keV. The differences are somewhat higher (<0.5%) between 1 keV and 5 keV due to the presence of the absorption edges.

e) Statistical analysis

The estimated variance s^2 on the mean value $\bar{x}$ of the variable x is calculated as $s^2 = \frac{1}{N(N-1)} \sum_{i=1}^{N} (x_i - \bar{x})^2$. The error is the square root of the variance. In MCNP, N is the total number of histories. The statistical uncertainty is computed for each particle on a history-by-history base.

The evaluation of the statistical uncertainty in EGSnrc is made at the end of the simulation using the matrices containing the results for each batch of particles. The variance s^2 is calculated by the same formula as in MCNP. The calculation of the uncertainty is however slightly different from the way it is implemented in MCNP as, in this case, it is computed per batch and not per history. N is the number of batches (no less than 10), x_i the result of batch i and $\bar{x}$ the average value for all batches.

2. Measurements

a) Phantom geometry

The measurements have been realised using micro-TLD of $1mm^3$ placed in phantoms made of solid water WT1, RW1 and in PMMA. Figure 35 shows the schematics of the two phantom geometries used during the measurements. The radial function geometry has been designed to minimize the interchip effect, so the TLD were placed on spiral arcs. Eight of these arcs were used so that for each session of measurements each point of measurement of the radial function was the result of 8 TLDs. The holes were cylindrical of 1.55 mm diameter and 1.1 mm depth. Those dimensions were large enough to allow the manipulation of the TLDs without friction, but small enough to avoid modification of the measurement due to the presence of air. The presence of the air around the TLD has been checked not to bring significant influence using specific Monte Carlo simulations where the dose to a TLD in water is compared to the dose to a TLD placed in a hole in water. The deduced differences are of the order of the statistical uncertainty of 0.5%.

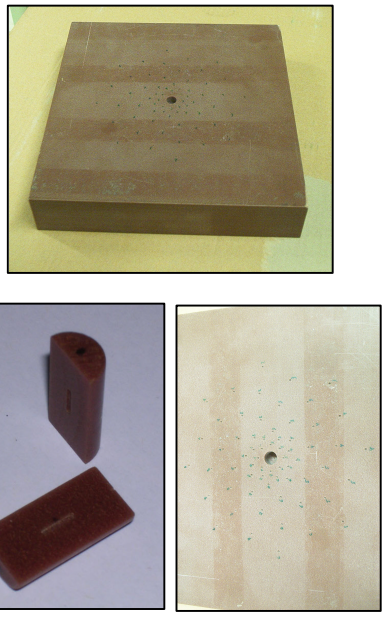

Figure 34: Pictures of the phantom and of the insert in WT1 used for the radial function measurements.

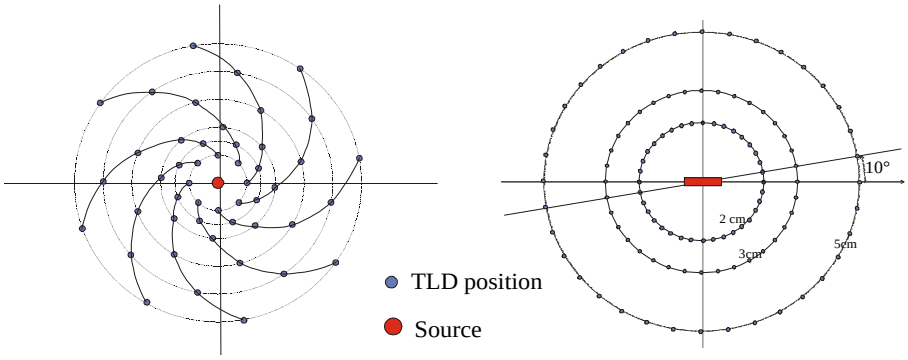

Figure 35: Schematic drawing of the phantom geometries: left for the radial function and right for the anisotropy function.

The distances chosen to measure the radial function are 1, 1.5, 2, 3, 4, 5, 6 and 7 cm. The anisotropy function was measured at 2, 3 and 5 cm with a TLD placed every 10°.

The central hole was made to accommodate a cylindrical insert containing the seed. This insert has been designed in order to avoid unnecessary manipulation of the radioactive source (see Figure 34).

b) TLD measurements

(1) TLD calibration

The detectors used in this work are TLD-100 LiF thermoluminescent microcubes of $1mm^3$ (Harshaw/Bicron 6801 Cochran Rd., Solon, OH 44139) (see Figure 36). The procedure for the external irradiation of the TLDs for calibration or other testing is always identical. We calibrated them using a 6MV linear accelerator (linac) (SL75 from Elekta) instead of the more classical ^{60}Co beam for convenience and because the variation in response of the TLD between ^{60}Co energy and 6 MV is very small. As a supplementary proof, the two values of the energy correction factor for the energy of the ^{125}I that we find in the literature are similar even if one was measured compared to a ^{60}Co beam and the other to a 4 MV linac. The linac is calibrated using a water phantom according to the protocol recommended by the NCS (Mijnheer et al. 1986) for high-energy photon beams. Prior to any irradiation, the linac output is verified using the local standard quality assurance procedure: in a polystyrene phantom using an ionization chamber placed at the depth of maximum dose (1.5 cm) at the centre of a $10x10cm^2$ field. During the irradiation with the external beam, the TLDs are placed at a depth of 3 cm in the same polystyrene phantom at the centre of a $20x20cm^2$ field. The size of the field has been chosen to avoid influence of the border of the field so that the TLDs are positioned in a region of the best uniformity. The dose variation across the field on the set was less than 1%. The TLDs were calibrated individually. After exposure sessions by the seeds, five “calibration TLD” of each batch were irradiated in the 6 MV field to correct for possible variation in the calibration factor of the TLD and for a possible instability of the reader. The entire batch was recalibrated when this correction exceeded 4%. The TLDs were selected to obtain a standard deviation on the measurements of 3.5%.

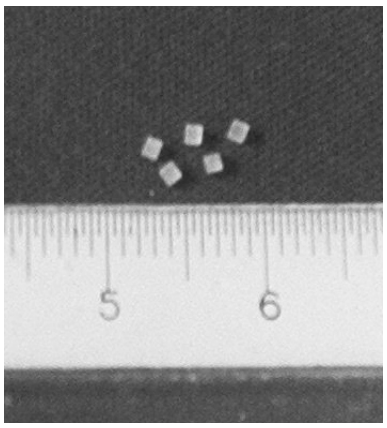

Figure 36: Picture of the $1mm^3$ TLD.

Prior to use, the TLDs are annealed. The procedure is to heat them at 400°C for one hour and at 100°C for 2 hours. There was always a delay of 24h between irradiation and readings in order to let the traps stabilize. The reading is performed in a Harshaw reader 3500. TLDs were first heated at 120C° for 25s to empty the unstable peaks, then to 250°C at a heating rate of 10°C/s (Yu and Luxton 1999). This procedure has been adopted because it permits to achieve a good reproducibility of the measurements.

Different correction factors were applied to obtain the dose rate in solid water per unit source strength from the TLD values, as described in equation (37) (Meigooni et al. 1995).

$$\frac{\dot{D}}{S_k} = \frac{R}{CF \times EF \times S_k \times t} \qquad \textbf{(37)}$$

In this equation R is the reading of the TLDs, *CF* is the calibration factor in terms of dose to water for the TLD response measured in the 6 MV beam, *EF* is the energy correction factor taken from the literature (see discussion in Chap III.B.2) to be 1.40 ± 5% for both isotopes (Meigooni et al. 1988), S_k is the source strength and t is the irradiation time corrected for the decay of the source by applying the formula $t = t_i . \frac{1 - \exp(-l\, t_i)}{l}$, where t_i is the real irradiation time. This can be deduced easily by replacing in equation 24 page 40 the kerma strength S_k by $S_k(t) = S_k(t_0)\exp(-l\, t)$, where λ is the decay constant, and integrating between t_0 and $t+t_0$. All the irradiations were in the linear response region of the TLDs, below 1Gy. Therefore, there was no correction for the supralinearity.

(2) Pre-testing of the 1mm^3 TLDs

For the measurements of the dosimetric functions around low energy photon emitters, it is important to use detectors allowing a high spatial resolution. Therefore, we have chosen to use very small TLDs of 1mm^3. These TLDs have first been tested to estimate their reliability.

During the measurements, 150 TLDs have been used. They were divided into 3 batches of 50 each. Within a batch, all the TLDs have undergone always the same thermal treatment, same number of reading cycles and annihilations, in order to preserve as much as possible the integrity of the batch.

Prior to the study, six of them have been irradiated using the 6MV beam with increasing doses from 0.25 to 1.5 Gy to verify their linearity. Figure 37 presents the results of these measurements. The regression coefficient is 0.9982, which is satisfactory. We have not investigated this linearity for higher doses, as, regarding the very low dose rate around the studied sources; it is already very unlikely to reach 1.5 Gy during the source measurements.

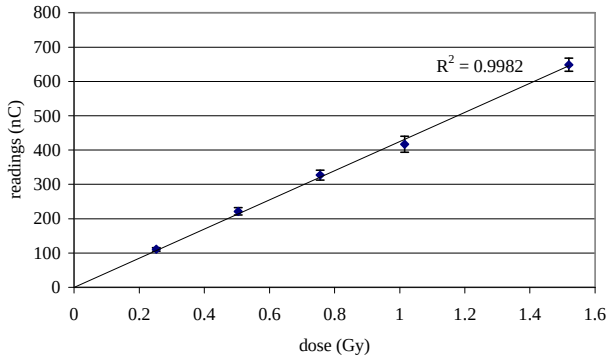

Figure 37: measured linearity of the 1mm^3 TLD between 0.25 and 1.5 Gy.

Figure 38 shows an example of the dispersion of the individual calibration factors measured for each TLD for one of the three batches. The mean standard deviation on 3 measurements for each batch is quite small, around or less than 2%, indicating that the reproducibility of the measurements is good. The small size of these TLDs induces however a high variability in the exact amount of material in each TLDs. That may explain the much larger spread of the calibration coefficients for these small TLDs compared to the bigger ones. Consequently, it was not possible to use a mean calibration factor per batch. We have chosen to use a specific calibration factor for each TLD based on, at least, 3 measurements.

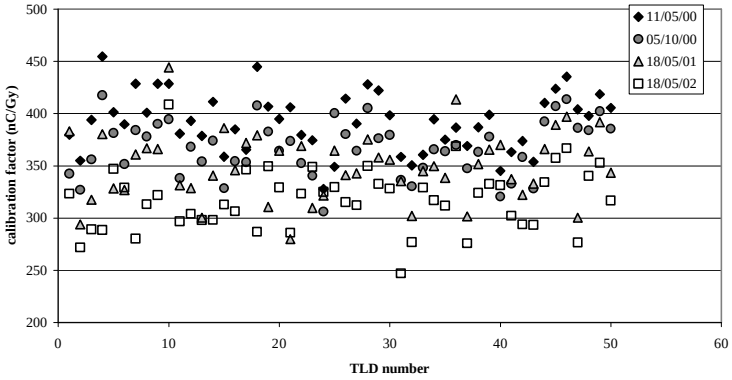

Figure 38: Dispersion of the individual calibration factors for each TLD of the batch n°3. Calibration factors from the 11/05/2000, 05/10/2000, 18/05/2001 and 18/05/2002 are displayed.

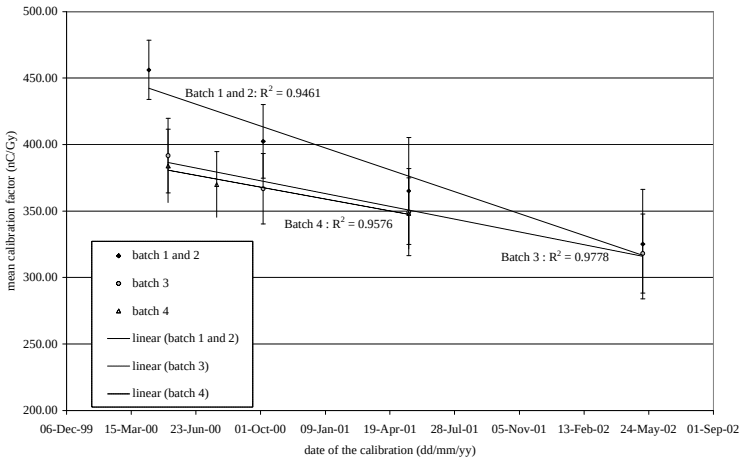

Figure 39 : Evolution of the calibration factors between March, 15 2000 and May, 24 2002.

One must also notice that the calibration factors vary significantly with time. Figure 39 shows the evolution of the mean calibration coefficient for each of the three batches between the beginning of the measurements in March 2000 and the end in May 2002. Over two years time, the TLDs of batch 2 and 3 have lost appreciatively 15 % of their initial sensitivity while those from the batches 1 and 2 have lost in the same time 25 % of their sensitivity. This loss of sensitivity has been previously reported as ~1% per reading for TLD-100 (Pla and Podgorsak 1983).

Regarding this relative instability of the calibration factors we have irradiated 24 hours before each reading 5 test TLDs at a known dose with the external beam. They were read together with the TLDs used for the measurements. A correction factor was deduced from these 5 readings. This procedure allows taking into account the decrease of the sensitivity of the TLDs but also the possible instability of the TLD reader. When this correction reached 4%, the whole batch was recalibrated.

Because of the very low dose rate of the IBt sources we had to measure very low doses. In order to check the validity of these measurements, 50 TLDs have been irradiated at a dose of 2 cGy. For this irradiation, the TLDs were placed as far as possible from the linac in a configuration used for Total Body Irradiation. The head of the linac is placed at 90° so that the beam is horizontal. The TLD were placed at a depth of 1.5 cm in a polystyrene phantom with a SSD of about 5.5 m. The field size was 20 x 20 cm². This configuration was chosen in order to use enough monitor units to assure the stability of the beam even for very low doses. The dose rate was measured in the condition of measurement using an ionization chamber. The dose rate measured in this configuration was 0.0376cGy/MU.

The calibration factor obtained in these conditions was within 2% of the factor measured with higher doses. This measurement was made in May 2002, two years after the first measurements of linearity and couldn't be shown in Figure 37 because the mean calibration factor had already drifted.

The fading has been studied on 10 TLDs over a period of 37 days. The total mean loss of dose was 3.8 cGy +/- 1.7 cGy. The loss per day is then 0.1 cGy +/- 0.04. Comparing these results with the mean dose received by the TLDs during the measurements and taking into account that the TLDs were always read within two days after the irradiation, we decided to neglect the influence of the fading in the following.

c) Water equivalence analysis

In parallel to the measurements, MC calculations have been performed in the three materials and in water. The water equivalence of the different media has been analysed in two different ways.

(1) Comparison of the dose rate constants

Even if the dose rate constant is officially defined only in water in the TG-43, it is possible to deduce an equivalent dose rate constant in each of the solid medium applying the following equation:

$$\Lambda_{medium} = \frac{\dot{D}(1cm,90°)}{K} \qquad \textbf{(38)}$$

The ratio between these dose rate constants for the media and the dose rate constant in water gives the correction factors to be applied on the measurements in order to obtain the value in water needed for clinical applications as recommended by the TG-43 of the AAPM. These dose rate constants in the solid media present the advantage that they can be calculated and also measured. The measurements are made using the TLDs placed at 1 cm during the measurements of the radial functions. The doses are calculated at 1cm in each phantom in a small element of water placed at 1cm on the transverse axis of the source. This takes into account the fact that the doses are measured using TLDs calibrated in dose to water and not dose to the medium. It is of course not possible to measure directly the dose in water. But the ratio between the measurements in the different solid can be used to check the validity of our MC simulations. These results have also been compared to the results of Luxton et al. (1994).

(2) Comparison of the radial functions

These solid phantoms are also used to measure the radial function and anisotropy function of seeds. It was interesting to verify the difference between radial functions calculated in solid media and radial function calculated in water in function of the distance from the seed. To validate our

calculations we have again used the ratio between the radial functions measured in the different media and compared them with our calculations.

d) <u>TLD perturbations</u>

Micro-TLD of 1 mm³ are small detectors compared to the mean free path of photons of 20 to 30 keV but are large compared with the range of the incident electrons. Consequently a large cavity theory must be applied. In that approach, the dose to the medium at a point *p* can be deduced from the dose to the detector at the same point *p* by:

$$D_{med}(p) = \overline{D}_{\det}(p) \times \frac{\int_{E_{\min}}^{E_{\max}} E[m_{en}(E)/r]_{med} (f_E)^p_{med}\, dE}{\int_{E_{\min}}^{E_{\max}} E[m_{en}(E)/r]_{\det} (f_E)^p_{\det}\, dE} \qquad \textbf{(39)}$$

where $\overline{D}_{\det}(p)$ is the average cavity or detector dose, $(f_E)^p_{med}$ is the photon fluence differential in energy E in the medium at the point p, $(f_E)^p_{\det}$ is the average photon fluence in the detector at the same point p and $[m_{en}(E)/r]_{med}$ and $[m_{en}(E)/r]_{\det}$ are the mass energy absorption coefficient at the energy E in the medium and in the detector respectively.

One can relate the photon fluence in the medium:

$$j_{med}(p) = \int_{E_{\min}}^{E_{\max}} (f_E)^p_{med}\, dE$$

to the photon fluence in the detector:

$$j_{\det}(p) = \int_{E_{\min}}^{E_{\max}} (f_E)^p_{\det}\, dE$$

through a perturbation factor $g(p)$ defined by:

$j_{med}(p) = j_{\det}(p) \times g(p)$.

However, it is usually assumed that the perturbation factor is equal to unity. In this case, $(f_E)^p_{med} = (f_E)^p_{\det}$. Introducing this in equation III-3, we can deduce that:

$$D_{med}(p) \approx \overline{D}_{\det}(p) \times (\overline{m}_{en}/r)_{med,\det}$$

$$\text{where } (\bar{m}_{en}/r)_{med,\det} = \frac{\int_{E_{nim}}^{E_{\max}} E[m_{en}(E)/r]_{med}(f_E)^p_{med}\,dE}{\int_{E_{\min}}^{E_{\max}} E[m_{en}(E)/r]_{\det}(f_E)^p_{med}\,dE} \qquad \textbf{(40)}$$

Monte Carlo calculations allow us to check the assumption that the perturbation factor is equal to unity for the case of low energy photons. Mobit et al. (1999) have published results of MC calculations showing that for 50 kV X-rays (equivalent to 29 keV photon) and for a 5 x 5 cm² field, the perturbation factor in LiF TLDs 1mm thick is no more than 1% at 1 cm depth. This means that the fluence is only slightly modified by the presence of the TLD. However, these authors acknowledge that this depends on the depth of the measurements and geometry of the beam.

Consequently, we have tried to evaluate the perturbation caused by the presence of the TLDs in our case. We have first calculated the radial function in the homogeneous medium, without the TLDs. Then, the radial function as measured by the TLDs was calculated by inserting 1 mm³ LiF cubes at the position of measurements on the transverse axis of the source, one at a time to avoid the shielding effect between the TLDs. The radial function was then calculated in the usual way. The ratio between the two radial dose functions gave us the perturbation factor introduced by the presence of the TLDs. This perturbation factor takes into account the slight variation in the ratio between m_{en}/r in LiF and in water with depth due to spectral modifications.

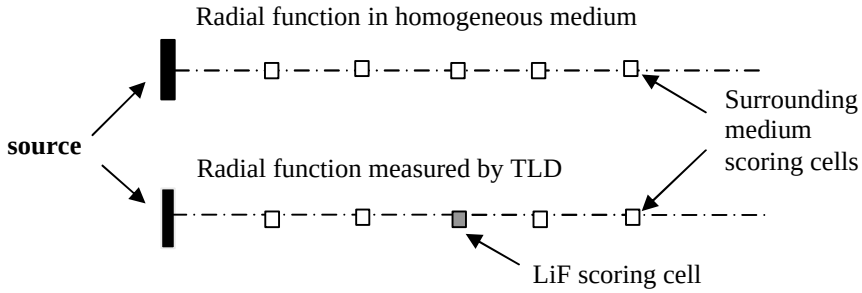

Figure 40: Method for simulating the TLD perturbation.

C. Dosimetric results

The results of the dosimetric part of this study can be grouped into several sections. The first section concerns the pure dosimetric data that are required for the use of the any new seed for clinical applications. It consists in the determination of the TG-43 parameters in water by measurements in solid media using TLDs and calculations using MCNP4, version B for the ^{125}I, upgraded to version C for ^{103}Pd and the following calculations. There is no difference concerning the photon transport between those two versions. These results have been published in two papers that are attached (pages 78 to 89, Reniers et al. 2001a, Reniers et al. 2002).

These first studies were performed using MCNP4B/C. Those results were then compared with new calculations performed using the EGSnrc MC code. This comparison between the radial functions was not satisfactory which implied new investigations (Reniers et al. 2001b). As was already mentioned, the only difference between those two codes that can introduce such discrepancies is in the interaction cross sections libraries they call upon. After careful examination of these data, the conclusion was that they effectively differ significantly below 50 keV for the photoelectric effect. The difference is large enough to explain the problem encountered for our seed simulations. This problem had been addressed during the same period by different authors (Bohm et al. 2003, Hobeila and Seuntjens 2003) who have modified the default cross sections of MCNP and EGSnrc in order to match newer cross section libraries, respectively, EPDL97 from Lawrence Livermore National Laboratory's (LLNL) and XCOM from National Institute of Standard and Technology (Hubbell and Seltzer 1995). Those authors have kindly accepted to allow us to use these updated libraries for the rest of our calculations. After this update, the two codes displayed a prefect agreement, within statistical uncertainty, even if the data were still not from the same origin, which is interesting to note.

However, the match with experimental data was still poor for large distances from the seed. To understand this, the perturbation introduced by the presence of the TLDs, that was neglected until then, has been investigated using MCNP4C with its updated cross sections. Following our study, a supplementary correction factor was introduced for the measured data which brought a very good agreement, within 5% of the calculated data nearly everywhere. The comparison between the codes and the agreement with the measured data has been published (Reniers et al. 2004) and is also attached in this chapter.

In parallel, the fact that we have used different solid media during the measurements has allowed us to compare those materials regarding their water equivalence for low energy photons. Those results are presented in section 3.

1. Dosimetric data

a) Validation of the procedure and results

As it was the first time we were working on the determination of dosimetric characteristics for seeds, it was important to test the procedure on a well known type of source, especially for the Monte Carlo calculations. The test seed was model 6711 from Amersham. It was modelled in MCNP using the geometry described by Williamson (1988). We have used for the measurements the same procedure as for the new type of seeds.

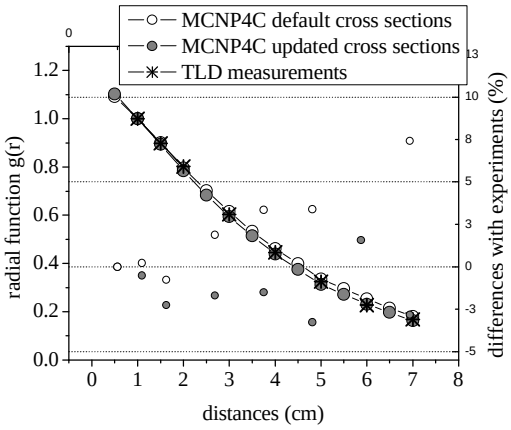

Figure 41: Radial dose function in WT1 measured with TLDs and calculated with MCNP4C using the default and the updated cross section libraries for model 6711.

The first dataset in Figure 41 (open symbols) were obtained with the default cross section of MCNP4B. Differences up to 8% with the measurements could be found above 4 cm distance. This kind of discrepancies was however commonly accepted in the literature, and still is. Later, we have redone the same calculations using the updated cross section data in MCNP4C. As is shown by the grey symbols in Figure 41, the agreement with the measurements is greatly improved.

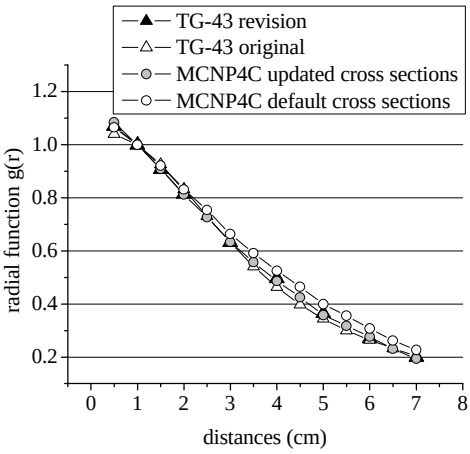

Figure 42: Radial function in water for model 6711.

The calculations were also performed in water and compared with the data of TG-43 (Nath et al. 1995). The results are shown on Figure 42. In the first comparison, the agreement with the TG-43 data was relatively poor (see open symbols). However, it was not really clear if the data from the report are in water or in

solid water WT1 as they are results of measurements but the method used for the eventual conversion into data in water is not mentioned. So, as the results of the comparison with the measurements were satisfactory, we have decided to move on with the simulation of the new sources. Later, we have also redone these calculations with the new cross section database and on the other hand, the data from the TG-43 were also revised (Rivard et al. 2004). The comparison between the new data (black and grey symbols) is clearly excellent, which is, with hindsight, a proof that the procedure was indeed correct.

As the calculations with EGSnrc were performed later and are clearly less straightforward to program, we have not validated those simulations for seed 6711. We have directly simulated the new seed models and validated it against our measurements in different materials.

A question was raised also concerning the need to model the organic matrix containing the active material. A detailed calculation including that supplementary layer of at most 0.0015 cm has been made using the MCNP code using the composition given by the IBt Company. However, as the difference on the results was not noticeable we have decided to ignore the organic matrix.

Dosimetric study of the new InterSource^{125} iodine seed

B. Reniers, S. Vynckier, Sc. PhD, P. Scalliet, M.D., PhD.
Cliniques Universitaires Saint-Luc,Service de Radiothérapie Oncologique,Université Catholique de Louvain,Brussels, Belgium.

Published in Medical Physics 28(11), 2001, pp 2285-2288

The use of low energy photon emitters for brachytherapy applications, as in the treatment of the prostate or of eye tumors, has significantly increased these last few years. New seed models for ^{125}I have been recently introduced. The aim of this study is to determine the dosimetric parameters as recommended by the AAPM in the TG43 formalism for a new iodine seed design: the InterSource^{125} (1). Measurements are made with LiF thermoluminescent dosimeters (size of 1mm ^{3}) in solid water phantoms to obtain the dose constant, the radial dose function and the anisotropy function. The TLD were calibrated at 6MV and an energy correction factor of 1.41 has been applied. The same dose parameters are also obtained by Monte Carlo calculations (MCNP4B) in solid water and in liquid water. The radial function was measured at 1, 1.5, 2, 3, 4, 5, 6 and 7cm and calculated between 0.3 and 7cm. The anisotropy functions were measured at 2, 3 and 5cm and calculated between 0.3 and 7cm.The calculated and the measured TG43 functions for solid water are in excellent agreement. We have then calculated these functions in liquid water to obtain the dosimetric information for clinical applications as per TG43 recommendations. In WT1, the calculated dose rate constant is 0.98+/-1% and the measured value is 1.03+/-7%. The calculated value for water is 1.02+/-1%.In conclusion, the dosimetric functions for the new iodine seed InterSource^{125} have been determined. They are quite different from the data of the well-known model 6711 from Amersham due to the absence of silver in the new seed. The characteristics are very similar to those of the model 6702.

The use of low energy photon emitters for brachytherapy applications, as in the treatment of the prostate or of eye tumors, has significantly increased these last few years. New seed models for ^{125}I have been recently introduced such as InterSource^{125} from the International Brachytherapy Company (IBt, SA Zone Industrielle C, Seneffe, Belgium 7180).

The new source is composed of two concentric titanium tubes of 0.04mm wall thickness, laser welded at the edges (see figure 1). On the inner tube is placed a 0.045mm thick Platinum/Iridium alloy x-ray marker (90% platinum and 10% iridium). The radioactive iodine is deposited on the inner tube as three printed bands of a thickness of 0.009mm for the central one and 0.015mm for the others. The active length of the source of 3.7mm was determined by the outer edges of the printed bands.

The sources are available with an air kerma strength between 0.254U and 1.27U, which corresponds to an apparent activity between 0.2mCi and 1.0mCi (7.4 MBq and 37 MBq). The air kerma strength is determined by the manufacturer by placing the sources in a reproducible way at a well-defined place in a Capintec CRC-7 well chamber. The calibration factor of this well chamber is traceable to the NIST 1999 standard (with the revision of 2000) through a calibration procedure using sources calibrated at NIST.

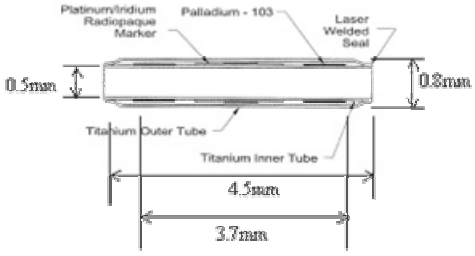

Figure 1: schematic drawing of InteSource^{125} from IBt

The dosimetric data have been obtained for this new seed according to the recommendation of the AAPM in the TG43[1] (1995), using the line source approximation with an effective source length of 3.7mm. In these recommendations of the AAPM, the dosimetric data must be determined in liquid water. However, the high dose gradients around the seeds make it very difficult to measure the doses directly in water. Therefore, to allow a precise positioning of the detector, measurements are performed in solid water phantom (i.e. WT1) using TLD dosimeters. The detectors are TLD-100 LiF thermoluminescent dosimeters of 1 mm^3 (Harshaw/Bicron 6801 Cochran Rd., Solon, OH 44139). Holes are drilled in the phantom corresponding exactly to the dimensions of the TLD's. The annealing procedure for the TLD is 400°C for one hour and 100°C for 2 hours. There was always a delay of 24h between irradiation and readings. They are read in a Harshaw reader 3500. TLDs were first heated at 120C° for 25s then to 250°C at a heating rate of 10°C/s. They are calibrated using a polystyrene phantom in a 6MV X-ray beam whose calibration was performed following the NCS calibration protocol[2].

The MCNP4B Monte Carlo code was used to calculate the TG-43 parameters in liquid water, after first verifying that the Monte Carlo calculations for solid water were in agreement with the measurements. In these calculations, in view of the low energy of the ^{125}I photons, the secondary electrons are assumed to deposit their energy locally, so only the photons were transported with a low energy cut-off of 1 keV; that implies also that the collision kerma in water closely approximates the absorbed dose. For the transport calculations, the interactions taken into account were Compton scattering with bounding effect, Rayleigh scattering and the photoelectric effect with emission of fluorescence photons, the detailed physics of MCNP4B[3]. The cross section data and the form factors for coherent and incoherent scattering are from Storm and Israel[4] or from ENDF[5] the fluorescence data are taken from Everett and Cashwell[6].

The seed geometry used in MCNP was as close as possible to the real one (see fig 1). We have used cylinders to model the core of the source and cones to model the swaged ends. The radioactive iodine, the emitting volume in the code, was positioned on the inner tube as in the real geometry, but, in view of the very thin emitting layer (max 0.015mm), and after verification, the presence of the organic matrix has been neglected.

The acquisition cells were defined by regions contained between cones and cylinders which axes were parallel to the source axis. Their volumes varied from 0.4mm^3 at 3mm from the source to 2.2cm^3 at 7cm. To calculate the average energy deposition in these cells, we have used the F6 tally[3]. For each calculation, 5,000,000 histories were used to obtain an error of less than 1% for the calculation on the transverse axis of the source. However, the statistical error in the dose is greater along the cylindrical axis because the seed emits fewer x-rays in that direction. At 5 cm from the seed center the computational statistical error on that axis is 14%.

We first validated our procedure with well-known models of iodine seeds, the models 6702 and 6711 from Nycomed/Amersham. For the radial function, the mean difference between our data and the data of the TG43 is less than 3% for both sources with a maximum of 5.5% at 4.5cm for 6702. The calculated dose rate constants were 1.021 (± 0.01) for 6702 and 0.976 (± 0.01) for 6711 instead of 1.04 and 0.98 respectively in the TG43. Considering the good results obtained with these sources, the same calculations were performed for the InterSource in WT1 and compared with the measurements with TLDs.

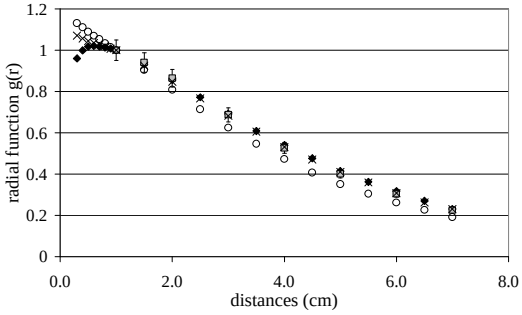

Figure 2: comparison between the calculations and the measurements for InterSource^{125} in solid water plastic WT1. The squares are the measurements and the diamonds are the calculations with MCNP4B. The error bars represent 1s (4%). The circles and the crosses are the calculated values for model 6711 and 6702 respectively.

For the radial function of the new source, the mean difference between the calculated and the measured function in solid water plastic WT1 is less than 2% (see figure 2). The same calculations were then performed for liquid water. The results are presented in the table I. The radial function obtained in water was fitted using a fifth order polynomial with a regression coefficient of 0.9993. The parameters are given in the table I and are usable up to 7cm in water. The error (1σ) on the relative measurements is 4%.

Figure 2 shows that the radial function of InterSource^{125} is closer to the radial function of model 6702. This is because the photons of model 6711 are less penetrating due to the presence of low energy x-rays characteristic of the silver used as marker in this model[7]. As there is no silver in the InterSource^{125}, the mean energy of the photons emitted by that seed (28.3keV at 3mm in air) is very comparable to the mean energy of model 6702 (28.3 keV) and a little bit more than for model 6711 (27.6keV). The values were calculated using the MCNP code. The mean values of the photon emission spectra presented by Luxton and al.[8] are 27.4 keV for model 6711 and 28.5 keV for model 6702.

	InterSource			
	solid water WT1		**liquid water**	
distance	**calculated**	**measured**	**calculated**	**fit**
0.3cm	0.960		0.938	0.958
0.4cm	0.999		0.980	0.975
0.5cm	1.017		1.000	0.988
0.6cm	1.020		1.006	0.998
0.7cm	1.017		1.010	1.004
0.8cm	1.013		1.009	1.007
0.9cm	1.008		1.004	1.007
1.0cm	1.000	1.000	1.000	1.005
1.5cm	0.932	0.943	0.953	0.964
2.0cm	0.856	0.864	0.891	0.893
2.5cm	0.772		0.813	0.812
3.0cm	0.692	0.702	0.738	0.732
3.5cm	0.608		0.662	0.657
4.0cm	0.540	0.526	0.591	0.591
4.5cm	0.476		0.525	0.529
5.0cm	0.414	0.411	0.469	0.472
5.5cm	0.362		0.415	0.415
6.0cm	0.317	0.303	0.362	0.361
6.5cm	0.270		0.315	0.311
7.0cm	0.230	0.217	0.273	0.275
fit coefficients		$a_0+a_1.r+a_2.r^2+a_3.r^3+a_4.r^4+a_5.r^5$		
R^2=0.9993		a0=	8.768E-01	+/-1.4E-2
		a1=	3.501E-01	+/-3.9E-2
		a2=	-2.894E-01	+/-3.2E-2
		a3=	7.588E-02	+/-1.1E-2
		a4=	-9.153E-03	+/-1.7E-3
		a5=	4.213E-04	+/-9.6E-5

Table I: radial function in solid water and liquid water for InterSource^{125}. Results of a polynomial fit for the radial function in liquid water.

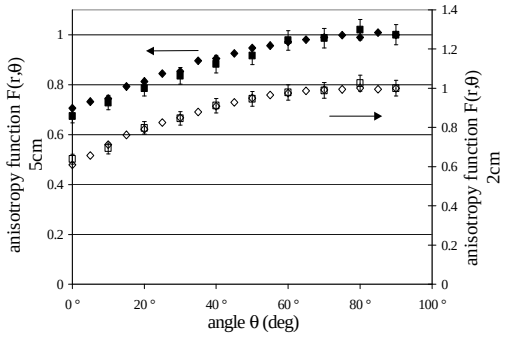

Figure 3: comparisons between calculations and measurements at 2cm (clear symbols) and 5cm (black symbols) for InterSource[125]. The squares are the measured values and the diamonds are the calculated values with MCNP4B. The error bars represent 1s (4%).

It is also interesting to note that for the new model, the maximum in the radial function, which is close to 0.5cm, is more pronounced than for the two other models. New Monte Carlo simulations were performed, modifying the location and amount of radioactive material and of the platinum marker. These calculations show that the different shape of the curve close to the InterSource[125] seed can be explained by the smaller amount of radioactive material on the center compared to the edges.

The anisotropy function for InterSource[125] was measured at 2, 3 and 5cm using TLDs in solid water WT1. The result of the comparison with the calculations (cf. figure 3) is very good with a mean difference of less than 3%. The maximum difference is on the axis of the source where the uncertainty on the calculations is high. For this reason, the same seed geometry has been used to calculate the anisotropy function in liquid water. The results are presented in the table II.

We note that the design of the InterSource[125] seed is quite different from other commercially available seeds (6702, 6711, MED3631-A/M[9, 10], I125-SL[11], isoSTAR[12]). The usual design is a tube of titanium sealed at each end; the thickness of the weld is typically about 0.5mm except for the model MED 3631-A/M where it is 0.15mm. For InterSource[125], there is also a thin weld of 0.1mm thick between the two cylinders. The attenuation in that weld is much lower than for the other sources so that we expected a flatter anisotropy function. This is confirmed in figure 4. Of the

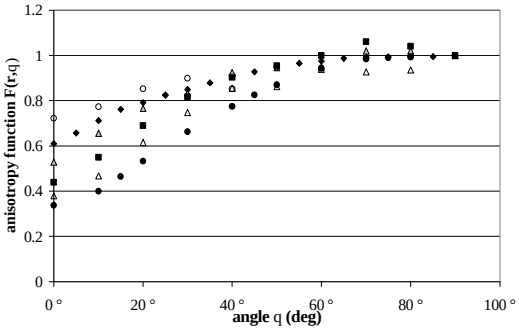

Figure 4: Anisotropy function at 2cm: comparison with other seed designs. The diamonds are the values for the InterSource, the squares represent the model 6711 (from TG43), the gray triangles are the data for model 6702 (from TG43), the circles are for isoSTAR model from Imagyn[12], the empty triangles are for model I125-SL [11] and the empty circles are for model MED 3631-A/M [9,10].

seeds we studied, the two sources with the flatter anisotropy functions are the sources with the thinner welds (InterSource and MED3631-A/M).

	Anisotropy function calculated in water				
q **(deg)**	**0.5cm**	**1cm**	**2cm**	**3cm**	**5cm**
0 °	0.515	0.554	0.656	0.681	0.703
5 °	0.697	0.637	0.659	0.714	0.718
10 °	0.781	0.711	0.712	0.737	0.752
15 °	0.831	0.764	0.769	0.780	0.798
20 °	0.863	0.795	0.792	0.811	0.818
25 °	0.888	0.827	0.823	0.841	0.845
30 °	0.910	0.860	0.852	0.860	0.854
35 °	0.934	0.881	0.880	0.891	0.897
40 °	0.956	0.909	0.912	0.912	0.911
45 °	0.973	0.931	0.928	0.933	0.935
50 °	0.988	0.952	0.948	0.950	0.954
55 °	0.999	0.967	0.965	0.970	0.959
60 °	1.003	0.983	0.972	0.976	0.968
65 °	1.005	0.990	0.984	0.985	0.979
70 °	1.003	0.990	0.991	0.996	0.988
75 °	1.006	0.998	0.993	0.997	0.988
80 °	1.003	0.996	0.997	0.995	0.988
85 °	1.003	0.998	0.996	0.996	1.000
90 °	1.000	1.000	1.000	1.000	1.000
f**an(r)**	**0.972**	**0.944**	**0.942**	**0.947**	**0.945**
f**an**	**0.950**				

Table II: Calculated anisotropy function of InterSource^{125} in water.

The dose rate constant was measured using 8 TLDs per measurement placed at 1cm from the source in solid water plastic WT1. The source air kerma strength was provided by the company and reported according to the NIST 1999 calibration (revision 2000). We used 4 different seeds with strengths between 1 and 2.5U.

To compare the experimental results with the Monte Carlo values, calculations were made in solid water. To calculate the dose rate constant, the kerma rate was first calculated at 5cm in air[13]. For that calculation, the cutoff of the photons was put at 4.6keV to suppress the titanium characteristic x-ray as in the NIST calibration[14]. We have used the inverse square law to deduce the kerma rate in air at 1cm from the center of the source, this result being equivalent to the source strength. Then the dose in water at 1cm from the center of the source on the transverse axis or in an element of water placed in the solid water phantom (to simulate the experiment with TLD calibrated in water) has been calculated. The ratio of

the two values gives us the "dose rate constant" of the source for each medium[13].

The dose rate constant is then calculated in liquid water. The ratio of these dose rates gives the correction factor necessary to transform the experimental data from a dose in solid water (WT1) into a dose in liquid water. The value of this ratio for InterSource^{125} is 1.031, which is close to the value obtained by Luxton et al. for model 6702: i.e. 1.025.

The measured value of the dose rate constant in water for the InterSource^{125} seed is 1.05 +/-7%. The calculated value is 1.02 +/- 1%.

In conclusion, the dosimetric characteristics of the model InterSource^{125} have been determined in water following the recommendations of the report of TG43. The dose rate constant and the radial function are quite close to those of the other sources without silver. The anisotropy function is slightly flatter than the function of other sources investigated due to the difference in thickness of the end closures of the seeds.

This work was supported by a grant from the Belgian "Fonds National pour la Recherche Scientifique" (F.N.R.S.). We wish also to thank N. Reyneart and H. Thierens from the Department of Biomedical Physics of the University of Gent (Belgium) for their help with the calculations using MCNP.

References

[1] Nath R., Anderson L.L., Luxton G., Weaver K.A., Williamson J.F., Meigooni A.S., "Dosimetry of interstitial brachytherapy sources: Recommendations of the AAPM Radiation Therapy Committee Task Group No. 43" Med. Phys. 22(2), pp. 209-234, Feb. 1995

[2] "Code of practice for the dosimetry of high energy photon beams" NCS report Dec. 1986

[3] "MCNP™ – A General Monte Carlo N-Particle Transport Code" Manual of the version 4B, J.F. Briesmeister, Editor

[4] E. Storm and H. I. Israel, "Photon Cross Sections from 0.001 to 100 Mev for Elements 1 through 100" Los Alamaos Laboratory report LA-3753, Nov. 1967

[5] J. H. Hubbell, W. J. Veigele, E. A. Briggs, R. T. Brown, D. T. Cromer and R. J. Howerton , "Atomic Form Factors, Incoherent Scattering Functions, and Photon Scattering Cross Sections" J. Phys. Chem. Ref. Data4, 471 (1975)

[6] C. J. Everett and E. D. Cashwell, "MCP Code Fluorescence-Routine Revision", Los Alamos Scientific Laboratory report LA-5240-MS, May 1973

[7] J. F. Williamson, "Comparison of measured and calculated dose rates in water near ^{125}I and ^{192}Ir seeds " Med. Phys 18(4), pp. 776-786, Jul./Aug. 1991

[8] G. Luxton, "Comparison of radiation Dosimetry in water and in solid phantom materials for ^{125}I and ^{103}Pd brachytherapy sources: EGS4 Monte Carlo study" Med. Phys 21(5), pp. 631-641, May 1994

[9] R. E. Wallace, "Report on the Dosimetry of a new design ^{125}Iodine brachytherapy source" Med. Phys 26(9), pp. 1925-1931, Sep. 1999

[10] Z. Li, J. J. Fan, J. R. Palta, “Experimental measurements of dosimetric parameters on the transverse axis of a new ^{125}I source” Med. Phys., 27(6), pp. 1275-1280, June 2000
[11] R. E. Wallace, “Dosimetric characterization of a new ^{125}Iodine brachytherapy source, model I125-SL”, *World Congress of Chicago 2000*, submitted to Med. Phys.
[12] R. Nath and N. Yue, “Dose distribution along the transverse axis of a new ^{125}I source for interstitial brachytherapy” Med. Phys 27(11), pp. 2536-2540, Nov. 2000
[13] A. S. Meigooni, K. Sowards and M. Soldano, “Dosimetric characterisctics of the InterSource103 palladium brachytherapy source”, Med. Phys., 27(5), pp 1093-1100, May 2000
[14] J. F. Williamson, “Monte Carlo evaluation of specific dose constant in water for ^{125}I seeds”, Med. Phys. 15(5), sep/oct 1988

Dosimetric study of a new palladium seed

B. Reniers, S. Vynckier, P. Scalliet

Cliniques Universitaires Saint-Luc, Universite Catholique de Louvain, Service de Radioth!erapie Oncologique, Bruxelles, Belgium

Received 1 March 2002; received in revised form 18 June 2002; accepted 25 June 2002

Published in Applied Radiation and Isotopes 57 (2002) 805-811

In this paper, the dosimetric parameters for a new palladium seed design: the InterSource[103,††] *are presented as recommended by the AAPM in the TG-43 formalism. Measurements are made with LiF thermoluminescent dosimeters (size of 1 mm*[3]*) in solid water phantoms WT1 to obtain the dose constant, the radial dose function and the anisotropy function. The TLD were calibrated at 6MV and an energy correction factor of 1.40 has been applied. The same dose parameters are also obtained by Monte Carlo calculations (MCNP4B) in solid water and in liquid water. The calculated and the measured TG-43 functions for solid water are in excellent agreement. In WT1, the calculated dose rate constant is 0.657 7 1% and the measured value is 0.672 7 7%. The calculated value for water is 0.69271%.*

The comparison with the previous study (Med. Phys. 27(5) (2000)) shows a very good agreement for the dose rate constant. The agreement for the radial function is poorer. For the measurements, it can be due to the difference of TLD settings. For the calculations the discrepancy could come from the different cross-section data utilized in the different Monte Carlo codes.

In conclusion, the dosimetric functions for the new iodine seed InterSource[103] *have been determined using the MCNP4B Monte Carlo code and TLD measurement in solid water WT1.*

Keywords: Brachytherapy; Dosimetry; Palladium[103], Monte Carlo simulation, MCNP4B

1. Introduction

The use of low-energy isotopes, like ^{125}I or ^{103}Pd, for the treatment of prostate, eye, or more rarely breast or cervix tumor, has increased during the last few years. The low energy of the ^{103}Pd photons, approximately 20 keV, results in a decrease in dose with distance more rapid than with other isotopes like ^{137}Cs or ^{192}Ir and even more than with ^{125}I and so diminishes the dose to the surrounding organs. Also, the

†† [1]Furnished by IBt, Seneffe, Belgium

short half-life, 17 days, results in higher dose rates than for ^{125}I. Palladium seeds currently constitute approximately a third of the permanent implant brachytherapy procedures.

As a consequence, the demand has increased and new types of seeds have become available for treatment use, such as the InterSource^{103} from the International Brachytherapy Company (IBt, SA Zone Industrielle C, Seneffe, Belgium 7180). The InterSource^{103} implants[‡‡] are hollow, hermetically sealed radiotherapeutic sources containing palladium-103 and a radiographic marker made of an alloy of platinum and iridium. The design is quite different from the previous models (e.g. models 200 from Theragenics). As per AAPM's TG-43 recommendations, prior to their clinical use, the dosimetric characteristics of these seeds must be carefully determined to provide reliable data for use in treatment-planning calculations and dose prescription.

The dosimetric data have been obtained according to the recommendation of the AAPM in TG-43 (Nath et al., 1995) for model InterSource^{103} from IBt. We have used the same protocol we had used for the InterSource^{125} (Reniers et al., 2001a, b). In the recommendations of the AAPM, these data must be determined in liquid water. However, the high dose gradients around the seeds make it very difficult to measure the doses directly in water. Therefore, measurements are performed in solid water phantoms using TLD dosimeters. These phantoms allow very precise positioning of the detectors. The dosimetric data in water have been determined using the MCNP4B Monte Carlo code, after verifying the code by comparing its prediction of the experimental measurements in the solid water phantom.

2. Materials and methods

2.1. Source description

The new source is composed of two concentric titanium tubes of 0.04mm wall thickness, laser welded at the edges (see Fig. 1). On the inner tube is placed a 0.045 mm thick platinum/iridium alloy X-ray marker (90% platinum and 10% iridium). The radioactive palladium in an organic polymeric carrier is deposited on the inner tube as three printed bands of a thickness of 0.009 mm for the central one and 0.015 mm for the others. The active length of the source of 3.7 mm was determined using the outer edges of the printed bands.

[‡‡] InterSource 125 is trademark of IBt SA. US patents #5,713,828, 6,086,942 and patents pending protect Inter-Source125 implants.

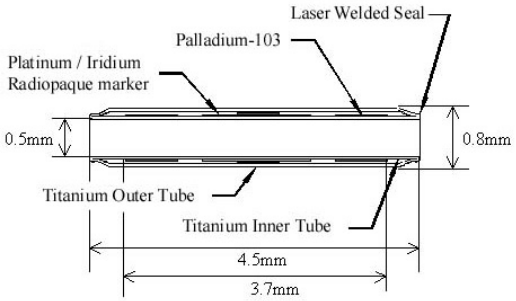

Figure 1: schematic drawing of InteSource[125] from IBt

The sources are available with an air kerma strength between 0.668 U[§§] and 2.67 U, or an apparent activity between 0.5 and 2.0 mCi (18.5 and 74MBq). The air kerma strength is determined by the manufacturer by placing the sources in a reproducible way in a Capintec CRC-15-R well chamber. The calibration factor of this well chamber is traceable to the NIST 1999 revised standard through a calibration procedure using sources calibrated at NIST.

2.2. Measurement

2.2.1. Detectors

The dose distribution around the source was measured using a solid water phantom WT1 (model 457, Radiation Measurement Inc., RMI, Middletown, WI). The detectors were TLD-100 LiF thermoluminescent dosimeters of 1mm3 (Harshaw/Bicron 6801 Cochran Rd., Solon, OH 44139). The annealing procedure for the TLD is 400°C for 1h and 100°C for 2 h. There was always a delay of 24 h between irradiation and readings. They were read in a Harshaw reader 3500. TLDs were first heated at 120°C for 25 s and then to 250°C at a heating rate of 10°C/s. They were calibrated using a polystyrene phantom in a 6MV X-ray beam whose calibration was performed following the NCS calibration protocol (NCS Report, 1986). The dose variation within the field on the set was less than 1%. After exposure sessions by the seeds, five calibration TLD of each batch were irradiated in the 6 MV calibration field to correct for possible variation in the calibration factor of the TLD and for an eventual instability of the reader. The entire batch was recalibrated when this correction exceeded 4%. The TLD were selected to obtain a standard deviation on the measurements of 3.5%. Different correction factors were used to obtain the dose rate in solid water per unit strength of the source from the TLD values, as described in the following (Meigooni et al.,1995):

$$\frac{\dot{D}}{S_k} = \frac{R}{CF \times EF \times S_k \times T} \qquad (1)$$

In this equation R is the reading of the TLDs, CF is the calibration factor of each TLD in the 6 MV beam, EF is the energy correction factor

[§§] cGy cm²/h

assumed from the literature (Meigooni et al., 1988) to be 1.40 7 5%, S_k is the source strength and T is the time of irradiation corrected for the decay of the source. All the irradiations were in the linear response region of the TLDs, below 1 Gy, so there was no correction for the supralinearity.

2.2.2. Phantoms

The distances of measurement for the radial function were 1, 1.5, 2, 3, 4 and 5 cm from the center of the source. The phantom, made of WT1, was designed to minimize the interchips effect (Meigooni et al., 1995). For the measurements of the anisotropy function, the TLDs were spaced at 10° intervals on a radius of 2, 3 and 5 cm from the center of the source. Circular holes with diameter of 1.5 mm and a depth of 1.1 mm were cut into the slabs of solid water. Contrary to previous determination the phantom was designed to use the same TLD of 1 mm^3 at all distances. Slabs of the same material were added where necessary so that there was at least 5 cm of solid water between any TLD and an exterior boundary of the phantom to provide full scattering conditions.

2.3. Calculations

As the AAPM (Nath et al., 1995) recommends obtaining the dosimetric characteristics for a new seed source in liquid water, Monte Carlo calculations are needed to transform the data from solid water into data in liquid water. The calculations for the dose distribution around the source were performed using version 4B of the MCNP.

The code MCNP4B (Briesmeister) is a general-purpose code that can be used for coupled neutron/ photon/electron transport. The code treats an arbitrary three-dimensional configuration of user-defined materials in geometric cells bounded by first- and second-degree surfaces and fourth-degree elliptical tori. The cells are defined by the intersections, unions and complements of the regions bounded by surfaces that are defined by supplying coefficients to the analytic surface equations or known points on the surfaces.

The cross-section data and the form factors for coherent and incoherent scattering are from Storm and Israel (1967) or from ENDF (Hubbell et al., 1975), the fluorescence data are taken from Everett and Cashwell (1973) (DLC189). For the low-energy photons, these data are different from the data of the XCOM library.

The dose distribution was first calculated in solid water WT1. The composition of the material is given in ICRU44 (1989) in percentage by mass: H: 8.1%, C: 67.2%, N: 2.4%, O: 19.9%, Cl: 0.1% and Ca: 2.3%. The geometrical modeling of the seed ends had negligible effect on the calculated radial function, $g(r)$, or the dose rate constant, L. But it does influence the anisotropy function, $F(r,q)$. It was found that modeling the conical section of the outer titanium tube with the conical geometry option available in MCNP results in a substantially better fit to the experimental data near zero degree, than calculations based on the conical sections modeled as multiple

cylinders. However, because the dose near zero degree is weighted by sin q, the end modeling has a nearly negligible effect (<1%) on the calculated anisotropy factor, $f_{an:}$ The calculations were then performed in liquid water as suggested in the TG-43 protocol.

To calculate the dose rate constant, the kerma per particle was first calculated at 5 cm in air (Meigooni et al., 2000), in both codes. For that calculation, the cutoff of the photons was put at 4.6 keV to suppress the titanium characteristic X-ray as in the NIST calibration (Williamson, 1988). We have used the inverse square law to deduce the kerma rate in air at 1 cm from the center of the source, this result being equivalent to the source strength. Then the dose in water at 1 cm from the center of the source on the transverse axis or in an element of water placed in the solid water phantom (to simulate the experiment with TLD calibrated in water) has been calculated. The ratio of the two values gives us the "dose rate constant" of the source for each medium (Meigooni et al., 2000).

3. Results

3.1. Radial function

The calculations were performed for the InterSource in WT1 and compared with TLD measurements (see Fig. 2). Fig. 2 shows the difference existing between the radial functions obtained by measurements and calculation. The differences between the TLD and the calculation are within 5%. We have also compared with the results presented by Meigooni et al. (2000). The differences between the measurements appear at 3 cm and are of the order of 15%.

It is interesting to note that we also can find the same kind of discrepancy for the measurements of the radial function of model 200 between the data of Meigooni et al. (1990), and the data of Sou-Tung Chiu-Tsao and Anderson (1991) (see Fig. 3a and b).

We suspect that this quite large difference could be related to the different sizes of the TLD used for the two series of measurements. Meigooni et al. use small TLD until 2 cm (included) and large TLD for greater distances to obtain a better sensitivity. Sou-Tung Chiu-Tsao and Anderson (1991) use large TLD everywhere, but they are placed perpendicularly to the measurement axes so that the attenuation thickness of the TLD to take into account for the radial function is only 0.89 mm. We use only small TLD. In the setup of Meigooni et al., the radial function for distances greater than 2 cm is a ratio between measurements obtained with large TLD and measurements obtained with small TLD.

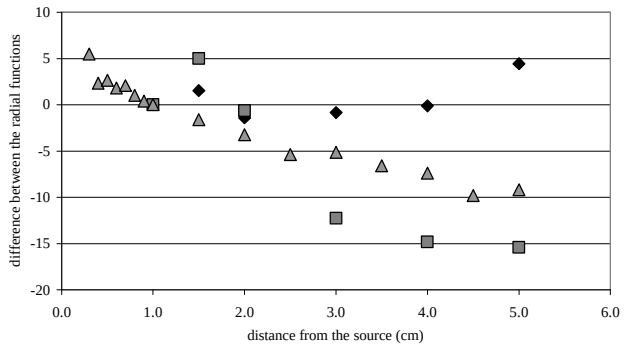

Figure. 2. Difference between the radial functions obtained by this team and the previous one. The lozenges show the difference between our measurements and the calculations with MCNP4B. The squares show the differences between the measurements of each team. The triangles are the differences between the calculations with MCNP4B and the measurements

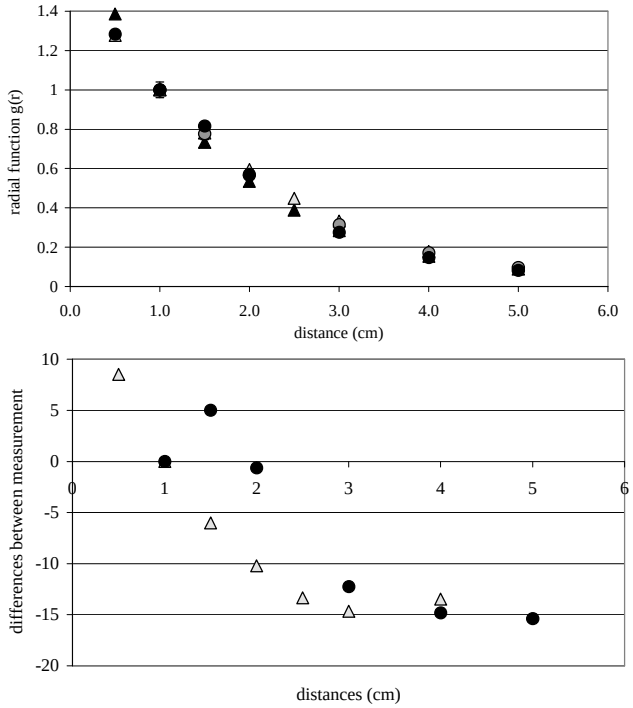

Figure. 3. (a) Comparison between the radial functions of model 200 (W) and of InterSource[103] (J). The black symbols are the measurements of Meigooni et al., the light symbols are the measurements of Sou-Tung Chiu-Tsao and Anderson (1991) for model 200 and the measurements of this work for the InterSource[103]. (b) Difference between the curves showed in Fig. 3a. The triangles are the differences between the results for model 200 and the circles are the differences for the InterSource.

Photons 20.7keV:	Attenuation	Ratio of the attenuation for the same thickness	Ratio of the perturbation for different thickness
0.5mm LiF =	0.892	1.08	1.17
0.5mm WT1 =	0.951		
1.55mm LiF =	0.710	1.26	
1.55mm WT1 =	0.887		

Table 1: Influence of the size of the TLDs

Radial function calculated in water				
Distances	**This work**	**Fit polynomial**	**Fit double exponentiel**	**Meigooni et al.**
0.3cm	1.216	1.240	**1.224**	1.247
0.4cm	1.236	1.222	1.225	1.241
0.5cm	1.212	1.197	1.207	1.214
0.6cm	1.179	1.167	1.177	1.195
0.7cm	1.136	1.132	1.139	1.160
0.8cm	1.089	1.094	1.096	1.104
0.9cm	1.044	1.053	1.050	1.051
1.0cm	1.000	1.011	1.004	1.000
1.5cm	0.787	0.794	0.782	0.777
2.0cm	0.610	0.603	0.600	0.589
2.5cm	0.464	0.458	0.459	0.443
3.0cm	0.352	0.354	0.351	0.327
3.5cm	0.266	0.276	0.268	0.246
4.0cm	0.202	0.208	0.205	0.180
4.5cm	0.151	0.147	0.157	0.134
5.0cm	0.113	0.121	0.120	0.098
Polynomial fit : $g(r) = a_0+a_1r+a_2r^2+a_3r^3+a_4r^4+a_5r^5$			*Double exponential fit :* $g(r) = a*\exp(-b*r) + c*\exp(-d*r)$	
$R^2 = 0.9994$			$R^2 = 0.9998$	
a_0 = 1.24369E+00 ± 3.249-02			a = 1.75978E+00 ± 2.956-02	
a_1 = 1.46998E-01 ± 1.134-01			b = 5.37182E-01 ± 7.177-03	
a_2 = -6.06276E-01± 1.299-01			c = -7.67547E-01 ± 4.897-02	
a_3 = 2.73537E-01± 6.281-02			d = 3.43270E+00 ± 3.665-01	
a_4 = -5.04927E-02± 1.332-02				
a_5 = 3.41110E-03± 1.022-03				

Table 2: Radial function calculated in water.

To obtain an approximation of the importance of this effect for 20 keV photons, we have calculated the ratio of the perturbation of the attenuation of the primary photons in the center of the region containing the TLD for the different TLD size (cf. Table 1).

This was confirmed by Monte Carlo calculations. We have calculated the ratio between the doses deposited in large LiF TLD and in small LiF TLD when their centers are placed at 2 cm from a palladium source. The result is a difference of 10% (74%).

The result of these quite simple calculations is consistent with the difference obtained in the radial functions and could reconcile the different measurements. The same calculations performed with Iodine source give a correction in the radial function measured with mixed TLD size of 5% for the distances where large TLD are used, which is of the same order as the experimental uncertainty.

We obtain also a difference between the calculations up to 10% at 5 cm. This could be related to the difference of cross-section data used in the two codes and will be analyzed in detail in another article (Reniers et al., 2001 b).

We have then used MCNP4B to calculate the radial dose function in water. These data have been fitted using a fifth order polynome and with a double exponential. They can be used up to 5 cm and are presented in Table 2. The double exponential gives a very good fit to the data with only four parameters. The errors on these parameters are also smaller than with the polynomial fit.

3.2. Anisotropy function

The anisotropy function for the InterSource^{103} has been measured at 2, 3 and 5 cm using TLDs in solid water WT1. The result of the comparison with the calculations (see Fig. 4a and b and Table 3) is very good with a mean difference of less than 3%. The maximum difference is on the axis of the source where the uncertainties of the calculations and of the measurements are high. Thus, the same seed geometry has been used to calculate the anisotropy function in liquid water. The results are presented in Table 4.

3.3. Dose rate constant

The dose rate constant has been measured using eight TLDs per measurement placed at 1 cm from the source in solid water plastic WT1. The source air kerma strength was provided by the company and reported according to the NIST 1999. We have used four different seeds with strengths between 1 and 3 U.

To compare the experimental results with the Monte Carlo values, calculations were made in solid water. The "dose rate constant" in solid water was calculated as explained in Section 2.3. The real dose rate constant is then calculated in liquid water (see Table 5). It is also possible to obtain the correction factor necessary to transform the experimental data from a dose in solid water

into a dose in liquid water. The calculated factor was 1.054. The value is consistent with the correction factor obtained by Luxton (1994) of 1.049 using EGS4.

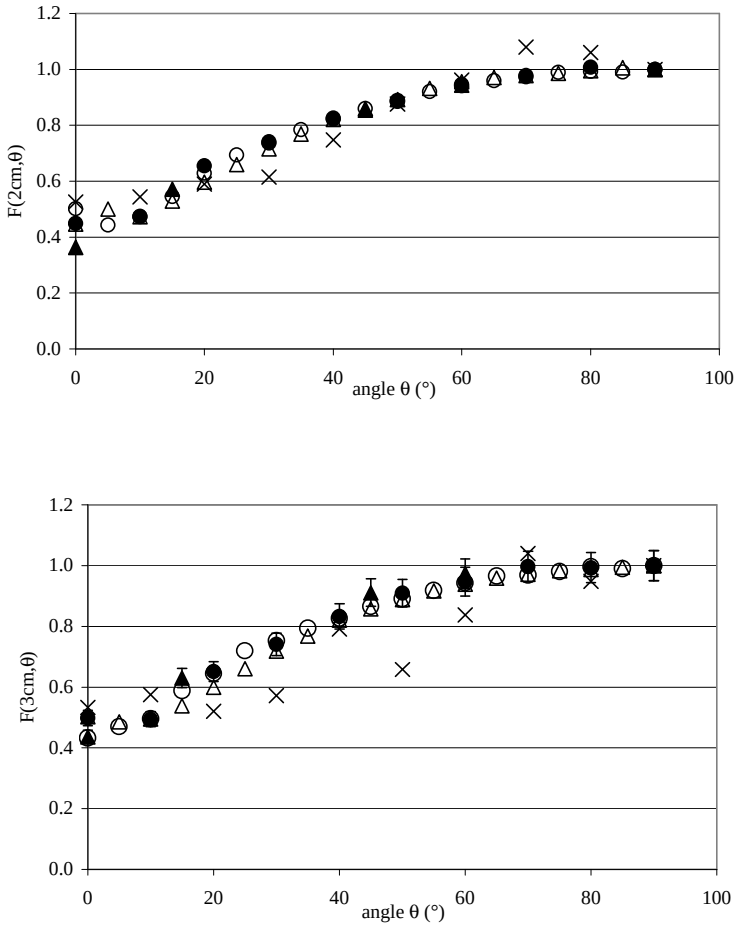

Figure 4: Anisotropy function for the InterSources[103] for 3cm (a) and 2cm (b). The circles are the results of this work, the triangles are the results of Meigooni et al.. Black symbols are for the measurements, light symbols are the calculations. The crosses are the corresponding anisotropy function for the model 200. The error bars represent 4% error (1s).

	Measurements in WT1			Calculations in WT1		
Angle (°)	**F(2cm,q)**	**F(3cm,q)**	**F(5cm,q)**	**F(2cm,q)**	**F(3cm,q)**	**F(5cm,q)**
0	0.456	0.498	0.514	0.392	0.432	0.462
5				0.402	0.470	0.504
10	0.464	0.494	0.551	0.461	0.496	0.520
15				0.547	0.588	0.599
20	0.641	0.651	0.671	0.619	0.645	0.641
25				0.681	0.720	0.699
30	0.737	0.741	0.757	0.721	0.752	0.767
35				0.758	0.794	0.801
40	0.810	0.833	0.829	0.799	0.827	0.827
45				0.835	0.866	0.863
50	0.879	0.909	0.885	0.875	0.891	0.890
55				0.907	0.918	0.926
60	0.932	0.947	0.923	0.933	0.943	0.961
65				0.955	0.965	0.970
70	0.964	0.997	0.949	0.968	0.969	0.969
75				0.982	0.980	0.999
80	1.004	0.993	0.985	0.994	0.996	1.004
85				0.991	0.990	0.975
90	1.000	1.000	1.000	1.000	1.000	1.000
F_{an}	**0.886**	**0.900**	**0.888**	**0.879**	**0.893**	**0.897**

Table 3: Anisotropy functions in WT1, measurements and calculations.

	Calculations in water		
Angle (°)	**F(2cm,q)**	**F(3cm,q)**	**F(5cm,q)**
0	0.392	0.415	0.442
5	0.402	0.451	0.482
10	0.461	0.477	0.498
15	0.547	0.566	0.575
20	0.619	0.622	0.617
25	0.681	0.696	0.674
30	0.721	0.730	0.742
35	0.758	0.773	0.778
40	0.799	0.807	0.806
45	0.835	0.849	0.845
50	0.875	0.877	0.874
55	0.907	0.906	0.913
60	0.933	0.934	0.951
65	0.955	0.959	0.962
70	0.968	0.964	0.964
75	0.982	0.978	0.996
80	0.994	0.995	1.003
85	0.991	0.989	0.974
90	1.000	1.000	1.000
F_{an}	**0.879**	**0.883**	**0.886**

Table 4: Anisotropy functions calculated in water.

The measured value of the dose rate constant in water for the InterSource^{103} seed is 0.708 ± 7%, the calculated value is 0.692. The results are presented in Table 5. Our results are very comparable with those of the previous team: 0.696.

	This work	**Meigooni**
L**(eau)**	0.692	0.696
L**(WT1) TLD**	0.657	0.664
L**(WT1) MC**	0.672	0.660

Table 5: Dose rate constant calculated in water and in WT1, and measured in WT1.

4. Discussion and conclusion

We have used the tally F6 of the MCNP code and LiF TLDs detectors in solid water WT1 from RMI to obtain the dosimetric data for the InterSource^{103} seeds produced by International Brachytherapy Company. Some authors[4] have pointed out that the cross-section tables used in MCNP4B are different from the XCOM cross-section database from Berger and Hubbell (1987) maintained at the National Institute of Standards and Technology (NIST) for the low-energy photons. It could be the cause of the discrepancy between our results and the calculations of the team of Meigooni et al., as they are using the DLC-099 library. To verify this possibility our team is performing these calculations with a third code (EGSnrc) and another cross-section library; this is part of an ongoing work and will be the object of a coming article.

Nevertheless, the radial function, $g(r)$ was measured at 1, 1.5, 2, 3, 4 and 5 cm in WT1 and calculated between 0.3 and 5 cm. The agreement between the calculations and the measurements is very good, within the experimental uncertainty everywhere. The error in the measurements is a little less than for the dose rate constant because $g(r)$ is a function relative to the dose at the reference point. For this measurement, the absolute calibration of the TLD (involving the energy correction factor) and the air strength calibration of the seeds cancel in the ratio of doses. The global error (1σ) is then 4%. The anisotropy function was measured every 10° at 2, 3 and 5 cm and calculated between 0.3 and 5 cm.

Regarding the measurements of the radial function, the 15% discrepancy with the previous team could be explained by the difference in the TLD setup. They used two different TLD sizes for the measurement of the radial function. As the attenuations in the TLD of 3.1 mm of radius and in the 1 mm TLD are not identical, especially for the 20keV photons, this could introduce an underestimation of the radial dose function on and after 3 cm. This should still be verified by measurement. The measured dose rate constant was found to be 0.708 ± 7%. It was obtained from measurements in solid water

transformed into measurements in water using a correction factor calculated with MCNP. The calculated value is 0.692 ± 1%. The dose rate constant value is very comparable with model 200. This is not surprising as the spectrum is not different between the two palladium seed models. The overall uncertainty on the measured dose rate constant in WT1 is assumed to be 7% with a standard deviation (1σ) on the repetitive measurements with the TLD (3.5%), the error on the calibration of the TLDs (2%), the error on the energy correction factor (5%), the error on the positioning of the TLD (1%) and air strength calibration of the seeds (3%) combined in quadrature.

In conclusion, the dosimetric characteristics of model InterSource^{103} have been determined in water following the recommendations of the report of TG-43. The dose rate constant, the anisotropy function and the radial function are quite similar to model 200.

Acknowledgements

This work was supported by a grant from the Belgian "Fonds National pour la Recherche Scientifique" (F.N.R.S.). We wish also to thank N. Reyneart and H. Thierens from the Department of Biomedical Physics of the University of Gent (Belgium) for their help with the calculations using MCNP.

References

Berger, M.J., Hubbell, J.H., 1987. XCOM: Photon Cross Sections on a Personal Computer NBSIR 87-3597. NBS,Washington, DC.

Briesmeister, J.F. (Ed.). MCNP^{t}—A General Monte Carlo N-Particle Transport Code. Manual of the version 4B. Everett, C.J., Cashwell, E.D., 1973. MCP code fluorescence routine revision. Los Alamos Scientific Laboratory Report LA-5240-MS, May 1973.

Hubbell, J.H., Veigele, W.J., Briggs, E.A., Brown, R.T., Cromer, D.T., Howerton, R.J., 1975. Atomic form factors, incoherent scattering functions, and photons scattering cross sections. J. Phys. Chem. Ref. Data 4, 471.

ICRU Report, 1989. Tissue substitutes in radiation dosimetry and measurement. ICRU Report 44, January 1989.

Luxton, G., 1994. Comparison of radiation dosimetry in water and in solid phantom materials for ^{125}I and ^{103}Pd brachytherapy sources: EGS4 Monte Carlo study. Med. Phys. 21 (5), 631-641.

Meigooni, A.S., Meli, J.A., Nath, R., 1988. A comparison of solid phantoms with water for dosimetry of ^{125}I brachytherapy sources. Med. Phys. 15 (5), 695-701.

Meigooni, A.S., Sabnis, S., Nath, R., 1990. Dosimetry of palladium-103 brachytherapy sources for permanent implants. Endocurietherapie/Hyperthermia Oncol. 6, 107-177.

Meigooni, A.S., Mishra, V., Panth, H., Williamson, J., 1995. Instrumentation and dosimeter-size artifacts in quantitative thermoluminescence dosimetry of low-dose fields. Med. Phys. 22(5), 555-561.

Meigooni, A.S., Sowards, K., Soldano, M., 2000. Dosimetric characteristics of the InterSource103 palladium brachyther-aphy source. Med. Phys. 27 (5), 1093-1100.

Nath, R., Anderson, L.L., Luxton, G., Weaver, K.A., William-son, J.F., Meigooni, A.S., 1995. Dosimetry of interstitial brachytherapy sources: recommendations of the AAPM Radiation Therapy Committee Task Group No. 43. Med. Phys. 22 (2), 209-234.

NCS Report, 1986. Code of practice for the dosimetry of high energy photon beams. NCS Report, December 1986.

Reniers, B., Vynckier, S., Scalliet, P., 2001a. Dosimetric study of the new InterSource^{125} iodine seed. Med. Phys. 28 (11), 2285-2288.

Reniers, B., Vynckier, S., Scalliet, P., 2001b. Dosimetric study of the new InterSource palladium and iodine seeds in different media. Radiother. Oncol. 61 (suppl. 1), S19.

Sou-Tung Chiu-Tsao, Anderson, L.L., 1991. Thermoluminescent dosimetry for ^{103}Pd seeds (model 200) in solid water phantom. Med. Phys. 18(3), 1991.

Storm, E., Israel, H.I., 1967. Photon cross sections from 0.001 to 100MeV for elements 1 through 100. Los Alamos Laboratory Report LA-3753, November 1967.

Williamson, J.F., 1988. Monte Carlo evaluation of specific dose constant in water for ^{125}I seeds. Med. Phys. 15(5), 1988.

INSTITUTE OF PHYSICS PUBLISHING PHYSICS IN MEDICINE AND BIOLOGY

Phys. Med. Biol. **49** (2004) 1569–1582 PII: S0031-9155(04)70686-7

The radial dose function of low-energy brachytherapy seeds in different solid phantoms: comparison between calculations with the EGSnrc and MCNP4C Monte Carlo codes and measurements

B Reniers[1], **F Verhaegen**[2] **and S Vynckier**[1]

[1] Cliniques Universitaires Saint-Luc, Service de Radiothérapie Oncologique, Université Catholique de Louvain, Bruxelles, Belgium
[2] Medical Physics Unit, McGill University, Montreal, Quebec, Canada

Received 16 October 2003
Published 24 March 2004
Online at stacks.iop.org/PMB/49/1569 (DOI: 10.1088/0031-9155/49/8/014)

Abstract

The use of low-energy photon emitters for brachytherapy applications, as in the treatment of the prostate or of eye tumours, has drastically increased in the last few years. New seed models for ^{103}Pd and ^{125}I have recently been introduced. The American Association of Physicists in Medicine recommends that measurements are made to obtain the dose rate constant, the radial dose function and the anisotropy function. These results must then be compared with Monte Carlo calculations to finally obtain the dosimetric parameters in liquid water. We have used the results obtained during the characterization of the new InterSource (furnished by IBt, Seneffe, Belgium) palladium and iodine sources to compare two Monte Carlo codes against experiment for these low energies. The measurements have been performed in three different media: two solid water plastics, WT1 and RW1, and polymethylmetacrylate. The Monte Carlo calculations were made using two different codes: MCNP4C and EGSnrc. These codes use photon cross-section data of a different origin. Differences were observed between both sets of input data below 100 keV, especially for the photoelectric effect. We obtained differences in the radial dose functions calculated with each code, which can be explained by the difference between the input data. New cross-section data were then tested for both codes. The agreement between the calculations using these new libraries is excellent. The differences are within the statistical uncertainties of the calculations. These results were compared with the experimental data. A good agreement is reached for both isotopes and in the three phantoms when the measured values are corrected for the presence of the TLDs in the phantom.

1. Introduction

The use of low-energy photon emitting isotopes, such as ^{125}I or ^{103}Pd, for the treatment of prostate, eye, or more rarely breast or cervix tumours, has increased during the last few years. The average photon energy of about 30 keV for ^{125}I and of about 20 keV for ^{103}Pd allows a more rapid decrease in dose with distance than with other isotopes such as ^{137}Cs or ^{192}Ir. Consequently, the dose to the surrounding organs is reduced. In addition, the short half-lives, 60 days for ^{125}I and 17 days for ^{103}Pd, allow the seeds to be used in permanent implants. The treatment of prostate tumours with ^{125}I has become one of the standard modalities in the United States and is presently gaining popularity in Europe.

Consequently, the demand for these isotopes has increased and new types of seed sources have become available for treatment use. According to the American Association of Physicists in Medicine (AAPM) recommendations in the TG-43 (1995) (Nath *et al* 1995), the dosimetric characteristics of such emitters must be determined in liquid water to provide reliable data for further use in treatment planning calculations and dose prescription. However, the high-dose gradients around these seeds make direct measurements of the doses in water very difficult. Therefore, these measurements are performed in solid water phantoms using TLD dosimeters; these phantoms allow a very precise positioning of the detectors. To obtain the data in liquid water, Monte Carlo (MC) simulations are mandatory.

Different MC codes are available, for example, the computer code developed by Williamson for brachytherapy sources, PTRAN (Williamson 1988, 1987), or different versions of EGS or MCNP. We have used two of the most recent codes to simulate two types of seeds: EGSnrc (Kawrakow and Rogers 2003) and MCNP4C (Briesmeister 2000). These two codes differ by their cross-section data and their geometry packages, and are not very well tested for low-energy brachytherapy sources. Comparisons between the calculations and the measurements are made for different water equivalent materials.

The seeds used in this study are the recently commercialized InterSource$^{125/103}$ models furnished by IBt[3]. The TG-43 analysis for these seeds has been achieved and published in previous papers (Reniers *et al* 2001a, 2002).

2. Materials and methods

Two MC codes, MCNP4C and EGSnrc, were used to simulate the dose distributions around two brachytherapy seeds of ^{125}I and ^{103}Pd in three different media. The seeds were the InterSource^{103} and the InterSource^{125} from IBt. Calculations and measurements were performed in WT1 (model 457, Radiation Measurement Inc., RMI, Middletown, WI), RW1 (PTW-Freiburg) and Polymethylmetacrylate (PMMA). One must recall that WT1 is the most frequently used material for measurements around brachytherapy sources even if RW1 has been proved to be more water equivalent for the photons emitted by ^{103}Pd and ^{125}I (Reniers *et al* 2001b, Luxton 1994). The use of three different phantom materials has given us more experimental data to test our calculations. The radial dose function, as defined below, was used as verification criterion for the dose distributions.

2.1. Dose formalism

The dose distribution around the seed, measured or calculated, was analysed using the well-known dose formalism recommended by the AAPM in the report of the TG-43 (Nath *et al*

[3] IBt, Seneffe, Belgium.

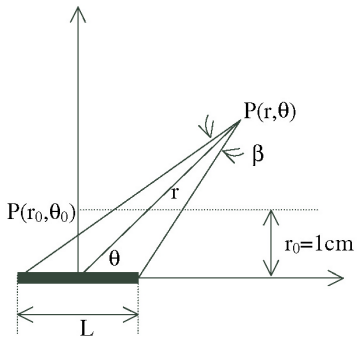

Figure 1. System of coordinates used for TG-43 formalism.

1995). This formalism is described in terms of a polar coordinate system (see figure 1). The reference point (r_0, θ_0) is chosen on the transverse axis at 1 cm from the centre of the source.

In this system, the dose rate at any point around the source can be expressed as

$$\dot{D}(r,\theta) = S_k \times \Lambda \times \frac{G(r,\theta)}{G(r_0,\theta_0)} \times g(r) \times F(r,\theta) \tag{1}$$

where S_k is the air kerma strength of the source (μGy m^2 h^{-1} or cGy cm^2 h^{-1}, also called U), Λ = dose rate constant = $\dot{D}(r_0,\theta_0)/S_K$, $G(r,\theta)$ = geometry factor = $\beta/(L \times r \times \sin\theta)$ for line source (see figure 1 for symbols), $g(r)$ = radial dose function = $\dot{D}(r,\theta_0)G(r_0,\theta_0)/\dot{D}(r_0,\theta_0)G(r,\theta_0)$ and $F(r,\theta)$ = anisotropy function = $\dot{D}(r,\theta)G(r,\theta_0)/\dot{D}(r,\theta_0)G(r,\theta)$.

The data were analysed using the line source approximation with a 3.7 mm active length for the geometry factor.

2.2. Measurements

2.2.1. Radial dose function measurements The description of the sources (i.e. InterSource models) and the methodology of the measurements applied in this paper have been detailed in previous papers (Reniers *et al* 2001a, 2002), so the description here will be brief.

The source design is presented schematically in figure 2. The InterSource seed is composed of two concentric titanium tubes in between which is a platinum/iridium alloy x-ray marker (90% Pt, 10% Ir). The ^{125}I or ^{103}Pd is deposited on the inner tube as three printed bands. The active length of the source of 3.7 mm is determined by the outer edges of the printed bands (cf figure 2).

The dose distribution around the source was measured in different solid water phantoms: WT1, RW1 and PMMA. The detectors were LiF thermoluminescent (TLD-100) microcubes of 1 mm^3 (Harshaw/Bicron 6801 Cochran Road, Solon, OH 44139). The annealing procedures for the TLD are 400 °C for 1 h and 100 °C for 2 h. There was always a delay of 24 h between irradiation and readings obtained from a Harshaw model 3500 reader. TLDs were first rapidly heated to 120 °C; that temperature was kept for 25 s for a pre-read anneal. The TLDs were then heated to 250 °C at a rate of 10 °C s^{-1} for the reading. They were individually calibrated using a polystyrene phantom in a 6 MV x-ray linear accelerator beam. The linear accelerator output was calibrated following the Nederlandse Commissie voor Stralingsdosimetrie (NCS) calibration protocol (Mijnheer *et al* 1986) in terms of absorbed dose to water before each

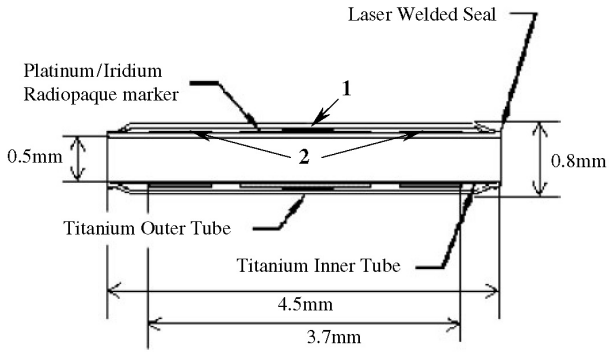

Figure 2. Schematic drawing of the InterSource$^{125/103}$ seed used in this study. 1 is the central emitting part of the source, 2 is the lateral emitting part of the source; the isotope can be ^{103}Pd or ^{125}I depending on the model.

irradiation of the TLD set. The dose variation across the field in which the detectors were set was less than 1%. After exposing the seeds, five 'calibration TLDs' of each batch were irradiated in the 6 MV field to correct for possible variation in the calibration factor of the TLDs and for a possible instability of the reader. The entire batch was recalibrated when this correction exceeded 4%. The TLDs were selected to obtain a standard deviation on the measurements of 3.5% or better. Several correction factors were applied to obtain the dose rate in phantom material per unit source strength from the TLD values, as follows (Meigooni *et al* 1995).

$$\frac{\dot{D}}{S_k} = \frac{R}{CF \times EF \times S_k \times T}. \tag{2}$$

In this equation R is the reading of the TLDs, CF the calibration factor for the TLD response measured in the 6 MV beam, EF the energy correction factor assumed from the literature (Meigooni *et al* 1988) to be $1.40 \pm 5\%$ for both isotopes, S_k the source strength and T is the time of irradiation corrected for the decay of the source. All the irradiations were in the linear response region of the TLDs, below 1 Gy. Therefore, no correction was necessary for the supralinearity effect.

The radial dose functions were measured at distances up to 5 cm for ^{103}Pd and 7 cm for ^{125}I. Cylindrical holes with a diameter of 1.5 mm and a depth of 1.1 mm were cut into the slabs of the different phantoms to accommodate the TLDs. Slabs of the same material were added where necessary so that there was at least 5 cm of solid water between any TLD and an external boundary of the phantom in order to provide full scattering conditions. The positions of the holes were selected to minimize the interchips effect (Meigooni *et al* 1995).

The overall uncertainty of the measurements of the radial dose function was estimated from the combination in quadrature of type A and type B uncertainties. The type A uncertainty is the standard deviation (1σ) on the repetitive measurements with the TLD (3.5%). The type B uncertainties for the radial dose function concern the calibration of the TLDs (2%) and the positioning of the TLD (1%). The combined uncertainty on the measured radial dose function points was estimated to be approximately 4.2%.

The presence of TLDs in the phantom for the measurements causes a perturbation; it modifies the fluence and the scattering of the low-energy photons compared to the homogeneous medium. In many studies, this perturbation is neglected. In this work Monte

Carlo calculations using MCNP4C were used to evaluate the perturbation effect on the radial dose function. For this purpose, we have simulated the measurement of the radial dose function, in the presence of the TLDs and compared it with the radial dose function calculated in a homogeneous medium. The TLDs are placed one at a time to avoid interchip effect; one calculation was performed for each position. For these calculations, only the central emitting part of the source was used (see figure 2). For the measurements, for practical reasons, the holes made to accommodate the TLDs are larger than the TLDs. However, during the calculations, the presence of the air around the TLD was not explicitly modelled as it had been checked that it does not significantly influence the dose in the TLD. The ratio of the calculations is used as a supplementary correction factor for the measurements and will be discussed in the results.

2.3. Monte Carlo calculations

The Monte Carlo calculations were performed using the version 4C of the MCNP code and version 3 of EGSnrc.

2.3.1. Description of the MC codes. The code MCNP4C (Briesmeister 2000) is a general-purpose code that can be used for coupled neutron/photon/electron transport. The code treats an arbitrary three-dimensional configuration of user-defined materials in geometric cells bounded by first- and second-degree polynomial surfaces and fourth-degree elliptical tori. The cells are defined by the intersections, unions and complements of the regions bounded by surfaces that are defined by supplying coefficients to the analytic surface equations or known points on the surfaces.

The distributed cross-section data and the form factors for coherent and incoherent photon scatterings are from the Storm and Israel library of 1967 (Storm and Israel 1967) or from ENDF (Hubbell *et al* 1975), the fluorescence data are taken from Everett and Cashwell (1973), report LA-5240-MS (DLC200). The photoelectric data are also from the Storm and Israel (1967) compilation. Bohm *et al* (2003) have compared the cross sections for the photoelectric effect of MCNP to the more recent data of National Institute of Standards and Technology's (NIST) (Hubbell and Seltzer 1995) and Lawrence Livermore National Laboratory's (LLNL) EPDL97 library. They show that MCNP cross-section data underpredict the value of the total cross section for low Z materials and low energies by as much as 7% at 20 keV. As can be seen in figures 3(b) and 4(b) (triangles), this difference is caused by discrepancies as high as 10% for 20 keV and 30 keV photons in the photoelectric data. That team then modified the MCNP library by replacing the original cross sections for the photoelectric effect by the EPDL97 library values up to 50 keV (see figures 3(b) and 4(b), circles). This modified library was used in this study.

The EGS (electron gamma shower) system of computer codes is a general-purpose package for Monte Carlo simulation of coupled transport of electrons and photons in an arbitrary geometry for particles with an energy above a few keV up to several hundreds of GeV. The cross-section data for the photoelectric effect are from the Storm and Israel library of 1970 (Storm and Israel 1970). The attenuation cross-section data, though closer to the NIST data (Hubbell and Seltzer 1995) than for the un-corrected MCNP data, were still not optimal, so an updated library (Hobeila and Seuntjens 2003) was used to compare the results of EGSnrc to the measurements (see figures 3(a) and 4(a)).

The following dosimetric quantities were scored in MCNP and EGSnrc for each particle as a function of distance from the source.

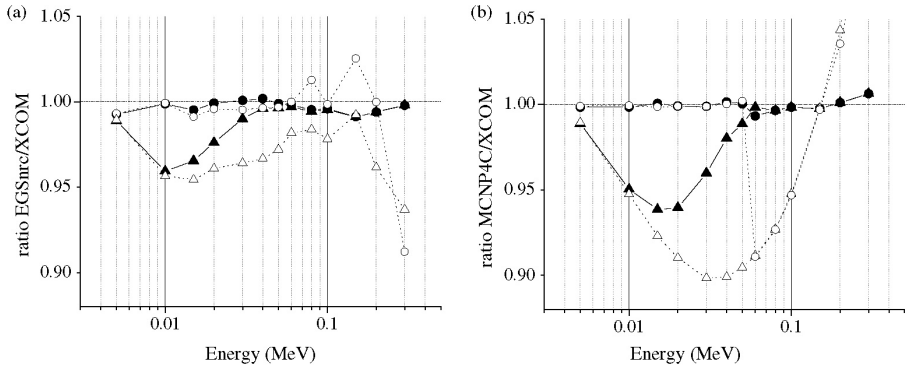

Figure 3. Comparison as a function of the photon energy of the mass attenuation coefficient, $\frac{\mu}{\rho}$, in water calculated with EGSnrc (a) and MCNP4C (b) MC codes and the mass attenuation coefficient, $\frac{\mu}{\rho}$, given by XCOM/NIST (Hubbell and Seltzer 1995). The triangles are the ratios between the original values of the codes and the XCOM/NIST coefficients and the circles are the ratios between the corrected cross-section data and the XCOM/NIST coefficients. The full lines and filled symbols correspond to the total attenuation, the dotted lines with open symbols to the photoelectric effect (lines are eye guides).

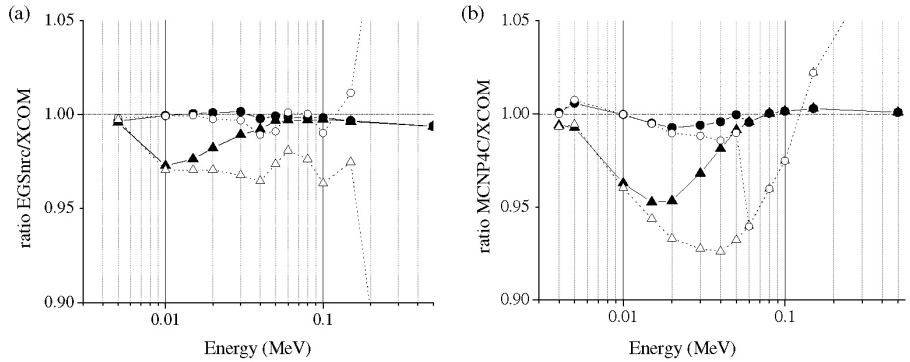

Figure 4. Comparison as a function of the photon energy of the mass attenuation coefficient, $\frac{\mu}{\rho}$, in WT1 calculated with EGSnrc (a) and MCNP4C (b) MC codes and the mass attenuation coefficient, $\frac{\mu}{\rho}$, given by XCOM/NIST (Hubbell and Seltzer 1995). The triangles are the ratios between the original values of the codes and the XCOM/NIST coefficients and the circles are the ratios between the corrected cross-section data and the XCOM/NIST coefficients. The full lines and filled symbols correspond to the total attenuation, the dotted lines with open symbols to the photoelectric effect (lines are eye guides).

Deposited energy

In MCNP4C: the pulse height tally $^*F8$, the asterisk meaning that the $F8$ tally is multiplied by the particle energy to give a result in MeV.

In EGSnrc: the parameter EDEP, which is the deposited energy.

Kerma for each particle

In MCNP4C: $F6 = W \times T_l \times \sigma_T(E) \times H(E) \times \rho_a/m$

where W is the particle weight, T_l the track length, V the volume of the cell, E the total particle energy, $\sigma_T(E)$ the microscopic total cross section at the energy E, $H(E)$ a heating number defined for the photons in MCNP by $H(E) = \sigma_T(E)\sum_{i=1}^{3} p_i(E) \times (E - \bar{E}_{\text{out}})$ with $p_i(E)$ the probability of reaction i (Compton scattering, pair production or photoelectric effect), $\bar{E}_{\text{out}}$ average exiting photon energy for reaction i, ρ_a the atom density (atoms/barns-cm) and m is the cell mass.

$$\text{In EGSnrc:} \quad K = \psi \times \mu_{\text{en}}(E) = \frac{\text{VSTEP} \times E(NP) \times WT(NP) \times \mu_{\text{en}}(E)}{V}$$

where K is the kerma, ψ the energy fluence, VSTEP the actual straight step length after truncation of the geometry, NP the stack pointer, E the total energy of the current particle, WT the weight of the current particle, V the volume of the cell and $\mu_{\text{en}}(E)$ is the mass-energy absorption coefficient taken from the XCOM distribution (Hubbell and Seltzer 1995). The data for RW1 are not directly available from XCOM, so to obtain the data for that material, we have used the XmuDat program (Nowotny 1998) freely distributed by the IAEA, which allows the calculation of the attenuation and of the energy absorption coefficients for any material between 1 keV and 50 MeV. This program offers the possibility of using the same library as the XCOM tabulation. However, we were obliged to use a fit for the $\mu_{\text{en}}(E)$ to determine the kerma in EGSnrc, which introduces an additional source of uncertainty. We calculated the fitting functions to keep the difference between the fitted values and the original data below 0.1% in the energy interval of 5 keV and 500 keV. The differences are slightly higher ($<0.5\%$) between 1 keV and 5 keV due to the presence of the absorption edges.

For the ^{125}I and ^{103}Pd low-energy photons, the secondary electrons were assumed to deposit their energy locally, so for these calculations only the photons were transported with a low-energy cut-off of 1 keV. This also implies that the collision kerma in the medium is equivalent to absorbed dose. However, the use of kerma calculations leads to smaller statistical uncertainties compared to energy deposition calculations, as it is not necessary that an interaction takes place in the cell to have a contribution to the tally. Unfortunately, to keep the consistency between the mass-absorption coefficients and the cross-section data used in the MC transport, it was possible to use kerma only for the calculations using the updated cross-section library. The radial dose functions calculated with the original libraries are obtained using dose calculations, so the uncertainties are slightly higher.

The interactions taken into account in the simulations were Compton scattering with electron binding effect, Rayleigh scattering and the photoelectric effect with emission of fluorescence photons. The dose distribution was calculated in water and in the three solid media: WT1, RW1 and PMMA. The compositions of the different media were taken from ICRU44 (International Commission of Radiation Units and Measurements (ICRU) 1989) in percentage by mass and can be found in table 1. The number of histories in the simulations was chosen to reduce the maximum statistical uncertainty for the Monte Carlo calculations, situated at 7 cm from the source to approximately 3%.

2.3.2. Geometries. For this study, the new seed model InterSource has the advantage of having an identical design for both ^{125}I and ^{103}Pd sources. We therefore used in MCNP and EGSnrc codes the same geometry for the two InterSource seeds but with a modified spectrum of the emitted photons. Cylinders were used to model the source core as well as the edges. It was verified (results not shown) that the presence of the conical shape of the end caps has a negligible effect on the dose on the transverse axis, so it was not necessary to model them for this study. The ^{125}I or ^{103}Pd layers, the emitting volume in the source model, were deposited on the inner tube as in the real geometry, but, in view of the extreme fineness of the emitting

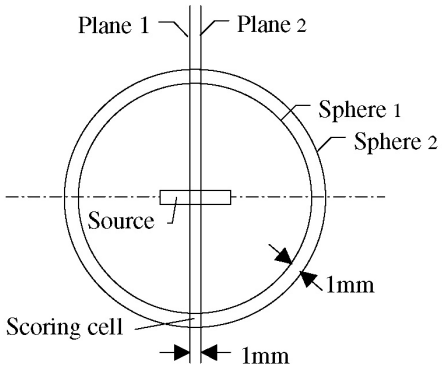

Figure 5. Schematic drawing of the scoring cells.

Table 1. Elemental compositions by percentage of weight, and mass density of the different phantom materials used in the study.

	WT1	RW1	PMMA	Water
H	8.1	13.2	8	11.2
C	67.2	79.4	60	–
N	2.4	–	–	–
O	19.9	3.8	32	88.8
Ca	2.3	2.7	–	–
Cl	0.1	–	–	–
Mg	–	0.9	–	–
Density	1.015	0.97	1.19	1

layer (max 0.015 mm) and after verification, the presence of the organic matrix containing the radioactive isotopes has been neglected.

The scoring cells, except for the evaluation of the TLD perturbation, were defined in MCNP and in EGSnrc codes by annuli on the transverse axis of the source defined by pairs of spheres spaced 1 mm apart, and two planes perpendicular to the source axis, also separated by 1 mm (see figure 5). For the calculation of the TLD perturbation, the source was kept unchanged, but the annuli were replaced by cubes of 1 mm^3 placed on the transverse axis of the source.

3. Results

We have used the MCNP4C and EGSnrc codes described above to calculate the radial dose functions of the two seeds and compare them with the experimental results. Figure 6 shows clearly that the results in water, which is the reference medium for clinical use, differ significantly from one code to the other. The radial dose function calculated with MCNP is up to 9% higher than with EGSnrc at 7 cm from an ^{125}I seed and 17% at 5 cm from a ^{103}Pd seed. These discrepancies result from a difference in the cross-section data. We then used the libraries modified to match EPDL97 in MCNP (Bohm *et al* 2003) and the NIST data in EGSnrc (Hobeila and Seuntjens 2003) and compared the new calculated results with the experimental values.

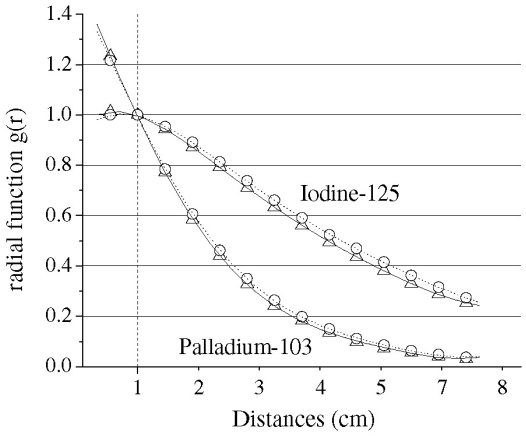

Figure 6. Radial function in water calculated with EGSnrc and MCNP4C using their original cross-section data. Open circles are for the MCNP4C code, full diamonds are for EGSnrc. Lines are polynomial fits of order 5.

3.1. Comparison of the cross-section data

The mass attenuation coefficients have been extracted from MCNP4C and EGSnrc codes and compared with the more recent data of the XCOM library distributed by NIST (Hubbell and Seltzer 1995). Two examples of these comparisons are given in figures 3 and 4 for water and solid water WT1. The differences in the total mass attenuation coefficients are mainly present in the region we are interested in, i.e. between 10 keV and 50 keV. As DeMarco *et al* (2002) have already pointed out, they can be as high as 7% in water for MCNP. The differences in the solid water plastics are a bit lower. The results for PMMA (not shown) are very similar to those for water. These discrepancies are mainly due to the photoelectric effect data, which can be up to 10% lower in the MCNP default database compared to the NIST database. For EGSnrc, the photoelectric data are much closer to the NIST data but could still be improved.

These improvements were made by Hobeila and Seuntjens (2003) for EGSnrc and Bohm *et al* (2003) for MCNP (see figures 3 and 4) by implementing new sets of cross sections. Figure 7 shows the radial dose functions in water calculated with these new sets. The remaining differences between the results obtained by the two codes are now within the statistical uncertainty which is of maximum 3%.

3.2. Comparison with experiment

We have compared these calculations with the measurements previously performed by our team to determine the TG-43 dosimetric characteristics of two new sources of ^{125}I and ^{103}Pd (Reniers *et al* 2001a, 2002). We have compared the calculations using the revised cross sections and the experiment in the case of the radial dose functions for the two sources in the three types of materials.

Figures 8 and 9 show the comparison between the measured radial dose functions and radial dose function calculated with both codes using the new cross-section data, respectively for WT1 and PMMA. The results of the comparison for RW1 are very similar to those for WT1 and are therefore not shown here.

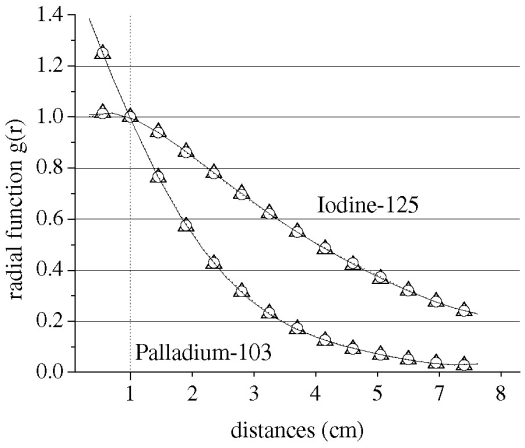

Figure 7. Radial dose function in water calculated with EGSnrc and MCNP4C using the modified cross-section data. Circles are for the MCNP4C code; triangles are for EGSnrc. Lines are polynomial fits of order 5.

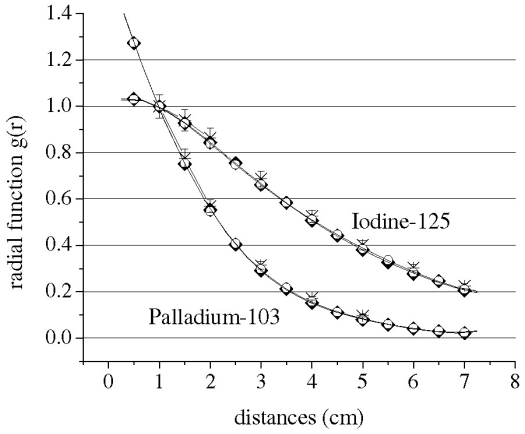

Figure 8. Comparison between calculation and experiment in WT1 for ^{103}Pd and ^{125}I. New cross-section data are used. Crosses are experimental data (±4%). Circles are for the MCNP4C code; triangles are for EGSnrc. Lines are polynomial fits of order 5.

For ^{125}I, the agreement between the two codes is greatly improved by the use of the new cross-section data. Differences are less than 3% up to 7 cm distance from the seeds in the three media, when it was up to 8% in WT1 and 10% in PMMA with the default libraries. The difference between the two codes for ^{103}Pd is improved too in the three media. With the default libraries, the discrepancies could reach more than 10% at distances larger than 5 cm from the seed in the three media. It is now less than 3% except at large distances, i.e. more than 5 cm for WT1 and 4 cm for PMMA, where it is still reduced to 5%. This remains a satisfactory result, as the statistical errors at these distances are still quite large for ^{103}Pd, up to 3%.

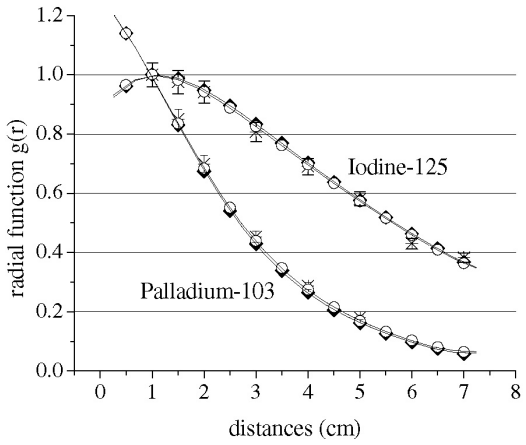

Figure 9. Comparison between calculation and experiment in PMMA for ^{103}Pd and ^{125}I. New cross-section data are used. Crosses are experimental data (±4%), open circles are for the MCNP4C code and diamonds are for EGSnrc. Lines are polynomial fits of order 5.

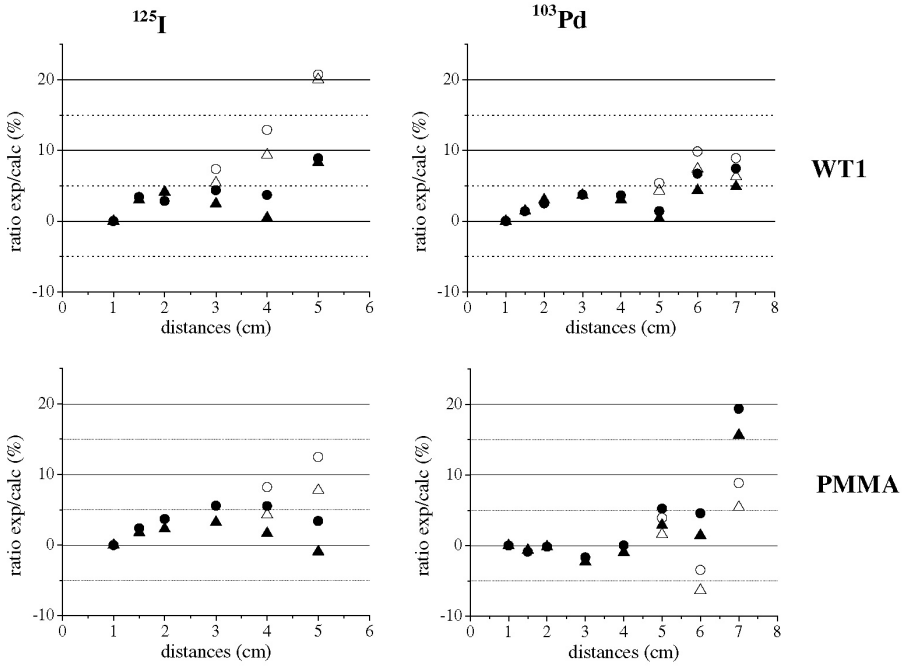

Figure 10. Differences between the measurements and the calculation with EGSnrc (circles) and MCNP4C (triangles). The open symbols are the comparison with the measurement without correction for the TLD perturbation; the full symbols are with the correction. Left figures are for ^{103}Pd and right figures for ^{125}I; the upper figures are for WT1, the lower for PMMA.

The agreement between measured values and calculations with the new cross sections is acceptable up to 5 cm for ^{125}I and up to 3 cm for ^{103}Pd. However, looking more closely

Table 2. Radial dose functions calculated for the central part of the source only, in the homogeneous medium and in the TLDs placed one by one in the medium at the position of the measurements.

Iodine									
	WT1			PMMA			RW1		
	$g(r)$	$g(r)$ TLD	Difference	$g(r)$	$g(r)$ TLD	Difference	$g(r)$	$g(r)$ TLD	Difference
0.5	1.116			1.047			1.106		
1	1.000	1.000	1.00	1.000	1.000	1.00	1.000	1.000	1.00
1.5	0.914			0.970			0.924		
2	0.824			0.925			0.844	0.833	1.01
2.5	0.735			0.870			0.761		
3	0.650	0.653	1.00	0.809			0.679		
3.5	0.572			0.745			0.602		
4	0.500			0.680			0.526		
4.5	0.433			0.618			0.465		
5	0.373	0.388	0.96	0.558	0.551	1.01	0.403	0.400	1.01
5.5	0.324			0.505			0.350		
6	0.279	0.287	0.97	0.450	0.416	1.08	0.305	0.321	0.95
6.5	0.238			0.397			0.263		
7	0.206	0.208	0.99	0.356	0.324	1.10	0.229	0.231	0.99
Palladium									
	WT1			PMMA			RW1		
	$g(r)$	$g(r)$ TLD	Difference	$g(r)$	$g(r)$ TLD	Difference	$g(r)$	$g(r)$ TLD	Difference
0.5	1.387			1.243			1.355		
1	1.000	1.000	1.00	1.000	1.000	1.00	1.000	1.000	1.00
1.5	0.738			0.820			0.754		
2	0.542			0.664			0.566	0.557	1.02
2.5	0.395			0.533			0.422		
3	0.287	0.296	0.97	0.425			0.314		
3.5	0.208			0.337			0.232		
4	0.150	0.163	0.92	0.264	0.271	0.97	0.171	0.184	0.93
4.5	0.108			0.208			0.125		
5	0.077	0.093	0.90	0.163	0.178	0.92	0.093	0.108	0.89
5.5	0.057			0.127			0.068		
6	0.041			0.099			0.050		
6.5	0.031			0.078			0.038		
7	0.023			0.063			0.030		

Radial functions calculated for the central source only; maximum uncertainty is 4% for Pd at 5 cm.

at the differences between the measurements and the calculations (see open symbols on figure 10), the results are poorer. For ^{125}I, the differences between experiment and calculations are within 5% up to 5 cm, and between 5 and 10% at 6 and 7 cm. But for ^{103}Pd, the differences at distances larger than 3 cm are quite large, up to 20% in WT1 at 5 cm.

To attempt to explain this discrepancy between measurements and calculations, the method used for measurement was investigated. The introduction of the TLDs in the medium constitutes a perturbation. A rough estimate of this perturbation factor can be obtained by considering the difference of attenuation between 0.5 mm (half a TLD) of TLD material and 0.5 mm of the surrounding medium using the attenuation coefficients. This difference is approximately 3% for photons of 30 keV in the three materials. It is approximately 8% for photons of 20 keV in the two solid water phantoms and approximately 8.8% in PMMA.

However, since the radial dose function is a relative function, mainly the ratio $\dot{D}(r)/\dot{D}(r_0)$, this correction for the simple attenuation of the primary photons largely cancels. That is why, at first, this perturbation was not taken into account.

In this work, we performed Monte Carlo simulations at some relevant distances to take into consideration not only the primary photon attenuation, but also the difference of scattering in the TLDs and the influence of the difference of steepness in the gradients moving farther from the source due to the approximate $1/r^2$ dependence of the dose. The radial dose functions calculated with MCNP4C (EPDL97) with the TLDs and without them are shown in table 2 for the central part of the source only. The ratios between these two radial dose functions have been used as a correction factor for the measurements. They were not equal to unity for distances larger than 3 cm, and can even reach 10% for ^{103}Pd. The filled symbols in figure 10 are the differences between the measurements corrected for the presence of the TLDs and the calculations. The differences between the calculated radial dose function and the measurements are within 5% nearly everywhere when the supplementary correction for TLD perturbation is applied.

4. Discussion and conclusion

There are many new types of brachytherapy seeds becoming available. Monte Carlo calculations are mandatory for the determination of their dosimetric characteristics as it is very difficult to perform measurements in liquid water. In this work, we have compared the results obtained for two types of brachytherapy sources using two different Monte Carlo codes. For the photons, the most important parameter that differentiated these codes in their original versions was their cross-section data libraries.

The comparison of the total attenuation coefficients in the three different media extracted from the original EGSnrc and MCNP codes confirms the differences in the photon cross-section data at low energy. We have compared the cross-section data of both codes with the XCOM library from NIST. In fact, both libraries differ from the more recent NIST data (Hubbell and Seltzer 1995). The difference for MCNP4C can reach 7% in water or PMMA and 5% for RW1 and WT1, mainly due to the photoelectric effect. Therefore, updated libraries (Bohm *et al* 2003, Hobeila and Seuntjens 2003) were used in both codes. The results calculated with the two codes using these new libraries are in very good agreement. This modification of the libraries makes the two codes equally adapted for calculation of dose distributions around low-energy photons brachytherapy sources.

This study also includes measurements of the radial dose functions around the seeds. The calculated results are also in good agreement with the experimental values when a correction factor for the TLD perturbation is applied to these measurements. This correction factor was calculated by Monte Carlo simulation and takes into account the perturbation induced by the presence of the TLDs in the phantom. The simple calculation of the attenuation of the primary radiation in the TLD alone was not sufficient to account for the effect of the TLD at these low photon energies, as it does not consider the difference in the scattering due to the TLDs or the variation in the steepness of the gradient between the TLDs close to the source and those very far away.

This work shows the importance of using updated cross-section libraries during the MC calculations, especially for low-energy photons, as this choice can introduce differences in the parameters used in clinical applications. It demonstrates too that for these very low energies, the presence of the TLDs during the measurements must be taken into account as a perturbation factor. The errors induced by neglecting this correction could be quite large, reaching 10% for ^{103}Pd.

Acknowledgments

This work was supported by a grant from the Belgian 'Fonds National pour la Recherche Scientifique' (F.N.R.S.). The authors wish also to thank Dr Tim Bohm from the University of Wisconsin for putting at our disposal the modified libraries for MCNP, Dr Jan Seuntjens from McGill University for the modified libraries in EGSnrc and for his advice and Dr Y El Masri from the Catholic University of Louvain and the referees for their valuable comments.

References

Bohm T D, DeLuca P M Jr and DeWerd L 2003 Brachytherapy dosimetry of ^{125}I and ^{103}Pd sources using an updated cross section library for MCNP Monte Carlo transport code *Med. Phys.* **30** 701–11

Briesmeister J F (ed) 2000 *MCNP—A General Monte Carlo N-Particle Transport Code* Version 4C LA 13709 (Los Alamos, NM: Los Alamos National Laboratory)

DeMarco J J, Wallace R E and Boedeker K 2002 An analysis of MCNP cross-sections and tally methods for low-energy photon emitters *Phys. Med. Biol.* **47** 1321–32

Everett C J and Cashwell E D 1973 MCP code fluorescence-routine revision *Los Alamos Scientific Laboratory Report* LA-5240-MS

Hobeila F and Seuntjens J P 2003 Effect of XCOM photoelectric cross-sections on dosimetric quantities calculated with EGSnrc *Proc. IAEA-CN-96–17*

Hubbell J H and Seltzer S M 1995 *Table of X-ray Mass Atomic Attenuation Coefficient and Mass Absorption Coefficient 1 keV to 20 MeV for Elements Z = 1 To 98 And 48 Additional Substances of Dosimetric Interest* National Institute of Standard and Technology, *NISTIR* 5632

Hubbell J H, Veigele W J, Briggs E A, Brown R T, Cromer D T and Howerton R J 1975 Atomic form factors, incoherent scattering functions, and photon scattering cross sections *J. Phys. Chem. Ref. Data* **4** 471–538

International Commission of Radiation Units and Measurements (ICRU) 1989 Tissue substitutes in radiation dosimetry and measurement *ICRU Report 44* (Bethesda, MD: ICRU)

Kawrakow I and Rogers D W O 2003 The EGSnrc code system: Monte Carlo simulation of electron and photon transport *Report PIRS-701* (Ottawa: National Research Council of Canada (NRCC)) (http://www.irs.inms.nrc.ca/inms/irs/EGSnrc)

Luxton G 1994 Comparison of radiation dosimetry in water and in solid phantom materials for I-125 and Pd-103 brachytherapy sources: EGS4 Monte Carlo study *Med. Phys.* **21** 631–41

Meigooni A S, Meli J A and Nath R 1988 A comparison of solid phantoms with water for dosimetry of ^{125}I brachytherapy sources *Med. Phys.* **15** 695–701

Meigooni A S, Mishra V, Panth H and Williamson J 1995 Instrumentation and dosimeter-size artifacts in quantitative thermoluminescence dosimetry of low-dose fields *Med. Phys.* **22** 555–61

Mijnheer B J, Aalbers A H L, van Gasteren J J M, Visser A G and Wittkämper F W 1986 Code of practice for the dosimetry of high energy photon beams *Nederlandse Commissie voor Stralingsdosimetrie (NCS) Report 2*

Nath R, Anderson L L, Luxton G, Weaver K A, Williamson J F and Meigooni A S 1995 Dosimetry of interstitial brachytherapy sources: Recommendations of the AAPM Radiation Therapy Committee Task Group No. 43 *Med. Phys.* **22** 209–34

Nowotny R 1998 XMuDat: photon attenuation data on PC version 1.0.1 online at http://www-nds.iaea.org/reports/nds-195.htm

Reniers B, Vynckier S and Scalliet P 2001a Dosimetric study of the new InterSource^{125} iodine seed *Med. Phys.* **28** 2285–8

Reniers B, Vynckier S and Scalliet P 2001b Dosimetric study of the new InterSource palladium and iodine seeds in different media *Radiother. Oncol.* **61** (Suppl. 1) S19

Reniers B, Vynckier S and Scalliet P 2002 Dosimetric study of a new palladium seed *Appl. Radiat. Isot.* **57** 805–11

Storm E and Israel H I 1967 Photon cross sections from 0.001 to 100 MeV for elements 1 through 100 *Los Alamos Laboratory Report* LA-3753

Storm E and Israel H I 1970 Photon cross sections from 0.001 to 100 MeV for elements $z = 1$ to $Z = 100$ *Atomic Data and Nuclear Data Tables* **7** 565–681

Williamson J F 1987 Monte Carlo evaluation of kerma at a point for photon transport problem *Med. Phys.* **14** 567–76

Williamson J F 1988 Monte Carlo simulation of photon transport phenomena *Monte Carlo Simulation in Radiological Science* ed R L Morin (Boca Raton, FL: CRC Press) pp 53–102

2. Water equivalence

a) Dose rate constant

The dose rate constants measured in different media are shown in Table 6. However, to convert the dose rate constants measured with TLDs calibrated in dose-to-water in a solid medium, to the clinically relevant dose rate constants in water, one needs to calculate the conversion factors using MC calculations. The dose rate constants in water as well as in different media have consequently been calculated and are listed in Table 6. To calculate these values, we need to calculate first the kerma in air at 1 cm from the source and the dose absorbed in a water cell at 1 cm from the source in the desired media, both per emitted particle. Table 7 shows these absolute results in air and Table 8, the absolute results in the water cells in different media. The first lines of both tables compare the results using the default cross-sections. The differences are quite high, ranging between 6% and 9% for both isotopes in air as well as in water. The similarity between the differences in water and in air explains why the values of the dose rate constants, which are ratios of these data, agree within experimental uncertainties with the measured ones (cf. Table 6).

^{103}InterSource	**MCNP values (+/-1%)**	diff calc-exp	**EGSnrc values (+/-1%)**	diff calc-exp	**exp (+/-7%)**
Λ(water)	**0.692**		**0.677**		
Λ(WT1)	**0.657**	-2.27 %	**0.646**	-3.86 %	**0.672**
Λ(RW1)	**0.682**	-0.75 %	**0.670**	-2.42 %	**0.687**
Λ(PMMA)	**0.827**	-0.76 %	**0.814**	-2.32 %	**0.833**

^{125}InterSource	**MCNP values (+/- 1%)**	diff calc-exp	**EGSnrc values (+/- 1%)**	diff calc-exp	**exp (+/-7%)**
Λ(water)	**1.009**		**1.002**		
Λ(WT1)	**0.979**	-4.95%	**0.976**	-5.26%	**1.03**
Λ(RW1)	**0.988**	-3.34%	**0.987**	-3.43%	**1.022**
Λ(PMMA)	**1.115**	-8.24%	**1.108**	-8.84%	**1.215**

Table 6: Dose rate constants calculated and measured in different media.

Palladium			Iodine		
default cross sections for both codes			**default cross sections for both codes**		
MCNP F6 (MeV/g.part)	**EGSnrc (MeV/g.part)**	**diff MCNP-EGSnrc (%)**	**MCNP F6 (MeV/g.part)**	**EGSnrc (MeV/g.part)**	**diff MCNP-EGSnrc (%)**
3.954E-04	4.317E-04	-8.41	2.480E-04	2.696E-04	-8.02
updated cross sections for both codes			**updated cross sections for both codes**		
MCNP F6 (MeV/g.part)	**EGSnrc (MeV/g.part)**	**diff MCNP-EGSnrc (%)**	**MCNP F6 (MeV/g.part)**	**EGSnrc (MeV/g.part)**	**diff MCNP-EGSnrc (%)**
4.160E-04	4.279E-04	-2.78	2.586E-04	2.760E-04	-6.29
MCNP F4*μ_{en} (MeV/g.part)	**EGSnrc (MeV/g.part)**	**diff MCNP-EGSnrc (%)**	**MCNP F4*μ_{en} (MeV/g.part)**	**EGSnrc (MeV/g.part)**	**diff MCNP-EGSnrc (%)**
4.221E-04	4.279E-04	-1.35	2.735E-04	2.760E-04	-0.90

Table 7: Kerma in air at 1 cm distance from the source. Comparisons between MCNP and EGSnrc prediceted results using the two sets of cross section data and two methods of tally for MCNP.

Palladium	**default cross sections for both codes**			Iodine	**default cross sections for both codes**		
	MCNP F6 (MeV/g.part)	**EGSnrc (MeV/g.part)**	**diff MCNP-EGSnrc(%)**		**MCNP F6 (MeV/g.part)**	**EGSnrc (MeV/g.part)**	**diff MCNP-EGSnrc(%)**
water	2.736E-04	2.921E-04	-6.32	**water**	2.503E-04	2.702E-04	-7.33
WT1	2.597E-04	2.789E-04	-6.88	**WT1**	2.428E-04	2.631E-04	-7.71
RW1	2.696E-04	2.894E-04	-6.83	**RW1**	2.450E-04	2.661E-04	-7.93
PMMA	3.268E-04	3.512E-04	-6.95	**PMMA**	2.765E-04	2.986E-04	-7.40
	updated cross sections for both codes				**updated cross sections for both codes**		
	MCNP F6 (MeV/g.part)	**EGSnrc (MeV/g.part)**	**diff MCNP-EGSnrc(%)**		**MCNP F6 (MeV/g.part)**	**EGSnrc (MeV/g.part)**	**diff MCNP-EGSnrc(%)**
water	2.735E-04	2.801E-04	-2.34	**water**	2.559E-04	2.733E-04	-6.34
WT1	2.677E-04	2.755E-04	-2.85	**WT1**	2.492E-04	2.655E-04	-6.14
RW1	2.796E-04	2.878E-04	-2.84	**RW1**	2.539E-04	2.711E-04	-6.35
PMMA	3.321E-04	3.358E-04	-1.10	**PMMA**	2.834E-04	3.024E-04	-6.28
	MCNP *F8 (MeV/g.part)	**EGSnrc (MeV/g.part)**	**diff MCNP-EGSnrc(%)**		**MCNP *F8 (MeV/g.part)**	**EGSnrc (MeV/g.part)**	**diff MCNP-EGSnrc(%)**
water	2.748E-04	2.801E-04	-1.89	**water**	2.687E-04	2.761E-04	-2.67
WT1	2.761E-04	2.755E-04	0.20	**WT1**	2.631E-04	2.655E-04	-0.91
RW1	2.892E-04	2.878E-04	0.49	**RW1**	2.679E-04	2.711E-04	-1.19
PMMA	3.435E-04	3.358E-04	2.28	**PMMA**	2.980E-04	3.024E-04	-1.44

Table 8: Absorbed dose to an element of water at 1 cm from the source in different media. Comparisons between MCNP and EGSnrc using the two sets of cross section data and two methods of tally for MCNP.

When we updated the cross sections data in both codes, but continued to use the F6 tally for MCNP (see Tables 7 and 8), the difference between the codes is reduced, but still quite high with nearly 3% for Palladium and more than 6% for Iodine in air and water, which is not expected for MC calculations with a statistical uncertainty less than 0.5%. A possible explanation, presently under investigation is that, contrary to what is done in EGSnrc, when we modify the cross sections data in MCNP, the heating factors, equivalent to the energy absorption coefficients, that are used in the calculations of the F6 tally are not also updated. So when that tally is used, even with the updated cross sections, there is still a systematic difference with the values calculated with EGSnrc, which uses consistent

cross section library and energy absorption coefficients. This problem can be solved easily in water or in the solid water materials by using the *F8 tally. That tally only scores the energy deposited inside a cell and is then only dependant on the cross sections libraries. Indeed, the discrepancy between the codes is reduced farther when using that tally (see Table 8). The remaining difference could be the result of the fit that had to be used for the energy absorption coefficients in EGSnrc and to the fact that the statistical uncertainty on the *F8 tally is higher. However, that technique of using *F8 is not possible in air because the dose scored is too low and the uncertainty much too high. So we have used the tally F4 that scores the energy flux in the cell. From MCNP calculations, we know the mean energy of the particles crossing the cell and so we can find the energy absorption coefficient for dry air in the XCOM distribution. The kerma in air is then calculated by $F4 \times m_{en}^{air}(E)$. Using that method, the agreement between the codes is very good (see Table 7).

Table 9 shows the results of the calculations with EGSnrc of the conversion factors (FC) in the different media. They are calculated as the ratios between the dose absorbed at 1cm on the transverse axis in water to the dose absorbed at 1cm on the transverse axis in an element of water in the medium. It compares the values before and after updating the cross sections data and compares it to the values published by Luxton et al in 1995 using EGS4 (Luxton 1994). As expected, with the default cross sections, the values we calculate agree extremely well, within half a percent, with those of the literature. However, as shown in Table 9, the values using the updated cross section do not agree anymore for Palladium. The new correction factors are generally lower or even reversed for RW1, with a correction of -2.5% instead of +1%. This could be expected as now the cross sections are different between our calculations and those of Luxton et al

Palladium

EGSnrc	default cross sections		updated cross sections		Luxton
	value	diff calc-litt (%)	value	diff calc-litt (%)	
CF (WT1)	1.047	-0.166	1.016	-3.102	1.049
CF (RW1)	1.009	-0.070	0.973	-3.646	1.010
CF (PMMA)	0.831	-0.182	0.834	0.123	0.833

Iodine

EGSnrc	default cross sections		updated cross sections		Luxton
	value	diff calc-litt (%)	value	diff calc-litt (%)	
CF (WT1)	1.029	0.421	1.027	0.175	1.025
CF (RW1)	1.008	0.104	1.015	0.812	1.007
CF (PMMA)	0.904	-0.366	0.905	-0.258	0.907

Table 9: Correction factors to apply to the dose rate constants measured in a solid phantom to obtain the dose rate constants in water. Calculations for both sources are performed with EGSnrc. The differences are in %.

As expected the correction factors needed to convert measurements of the dose rate constants in PMMA into dose rate constants in water is very high, 0.90 for ^{125}I and 0.83 for ^{103}Pd. For the two solid water materials, these factors are much smaller, with only at most 2.9%.

b) Radial function

The other dosimetric parameters, radial function and anisotropy function were also measured in solid materials instead of water. Figure 43 presents the ratio of the radial function calculated in the solid media to the radial function calculated in water for Iodine and Palladium seeds.

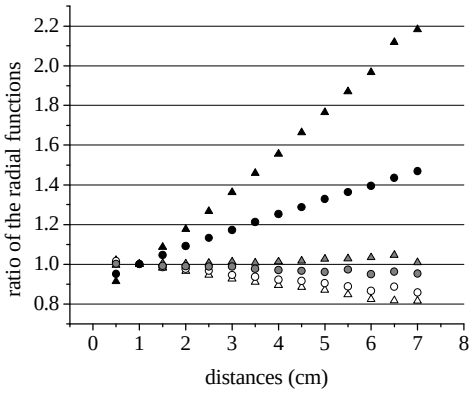

Figure 43 Ratio between the radial function calculated in medium and the radial function calculated in water. Circles are for Iodine and triangles for Palladium. Black is PMMA/water, grey is RW1/water and white is WT1/water.

The measurements of the radial function in PMMA introduce differences of more than 75% at 5 cm for ^{103}Pd and 30% for ^{125}I. The differences introduced by using the two solid water plastics are lower but still quite important for WT1 (up to 15%). RW1 on the contrary has been engineered to be used for low energy photons; the radial functions measured in this plastic for ^{125}I and ^{103}Pd are quite close to the radial functions calculated in water for the two isotopes (< 5% up to 7 cm distance from the source).

To check the calculations, we have used the measurements in different media, as shown in Figure 44. In this figure the ratios of the radial functions calculated in PMMA to the radial functions calculated in WT1 are compared to the measured values of these ratios. The correspondence is good for both codes.

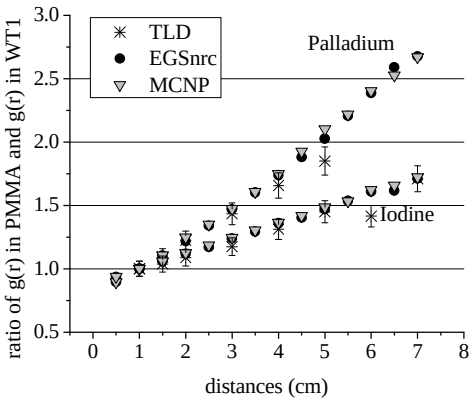

Figure 44: Comparison with experiment of the ratios of g(r) in PMMA to g(r) in WT1 calculated with EGSnrc (black points) and MCNP4C (open triangles).

c) Corollary: tissue equivalence of water?

To go one step further in this study of equivalence between media, we have compared the radial dose functions calculated in these solid water materials and in water and radial functions calculated in natural tissues as muscles or eye lens tissue for Palladium and Iodine (Figure 45) and for photons of 300 keV (Figure 46). The compositions used for the tissue media is taken from ICRU 44 (1989) and are listed in Table 10.

If for photons of 300 keV the radial function in water is completely equivalent to the radial function in muscle, it is less true for photons of 20 or 30 keV. The radial function obtained in muscles is more comparable to the one obtained in solid water WT1 than in water. On the contrary, for eye lens, it is effectively the same radial function as in water. Even if the densities and the content of H, C, N and O are quite similar for muscle and eye lens, the muscle contains slightly more high Z elements with the presence of Potassium (Z=19). This could perhaps explain the observed difference between the radial functions.

medium	H	C	N	O	others	ρ (kg m^{-3})
Muscle (skeletal)	10.2	14.3	3.4	71.0	0.1 Na, 0.2 P, 0.3 S, 0.1 Cl, 0.4 K	1050
Eye lens	9.6	19.5	5.7	64.6	0.1 Na, 0.1 P, 0.3 S, 0.1 Cl	1070
WT1	8.1	67.2	2.4	19.9	2.3 Ca, 0.1 Cl	1015
RW1	13.2	79.4		3.8	2.7 Ca, 0.9 Mg	970
PMMA	8	60	32			1190
water	11.2			88.8		1000

Table 10: Elemental compositions of the different medium used in the comparison (see text) (ICRU 44).

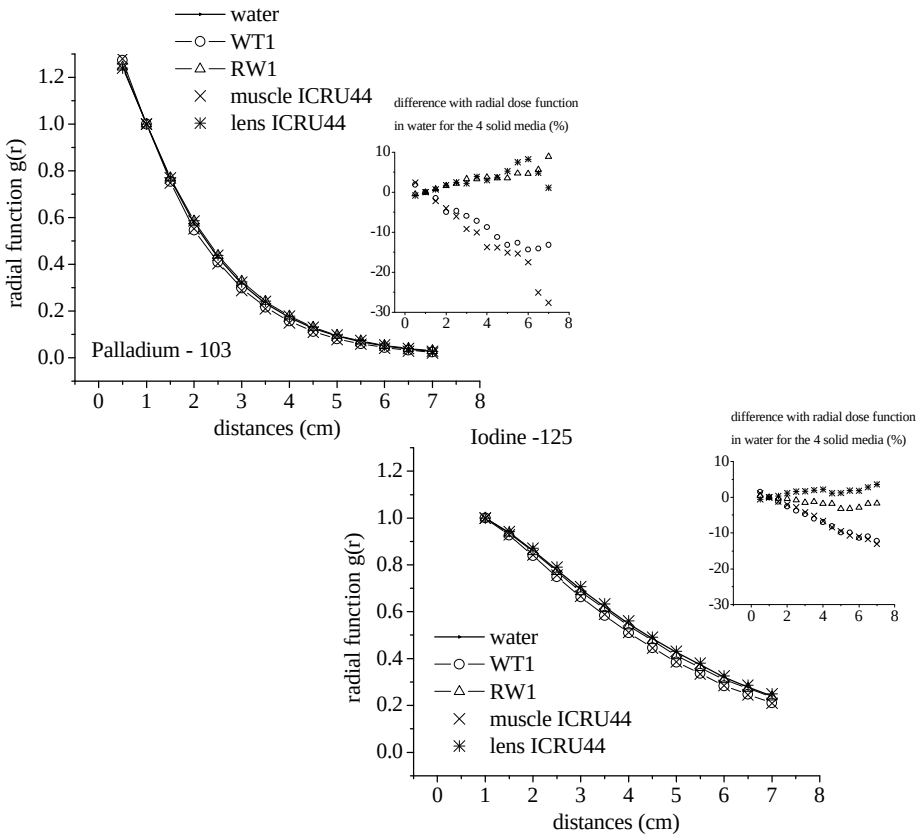

Figure 45: Radial functions in different media for Palladium-103 (left) and Iodine-125 (right).

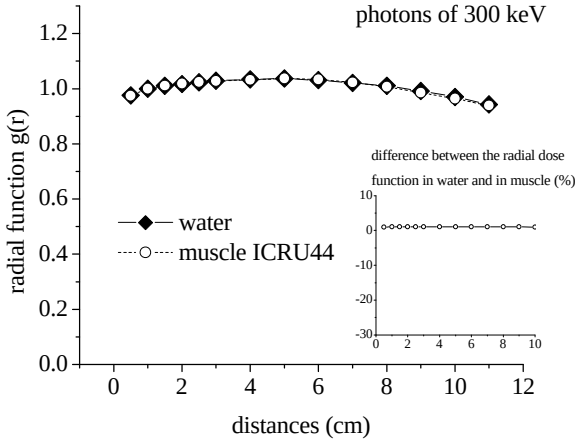

Figure 46: Radial function of a point source of 300 keV in water and in ICRU skeletal muscle.

d) Conclusion about water equivalence

The equipment classically used for dose measurements is calibrated in terms of dose-to-water. When treatment planning systems were based only on measured data, the only possibility was consequently to use dose-to-water, even for heterogeneous media. In this case, some corrections are made to take into account the difference in attenuation or in scattering, but the resulting absorbed dose is always dose-to-water, which means the dose to a small volume of water inside the medium. When Monte Carlo calculations have been introduced, it gave the possibility for the first time to calculate the actual dose to the medium, which differs from dose-to-water by the ratio of the mass energy absorption coefficients. This introduces a complication when one tries to compare different media as it is always questionable to compare dose in different media. First of all is it really comparable? What does it mean for the patient? How can it be interpreted in a context where all the expertise is based on dose-to-water? So we have chosen to continue to use the dose-to-water for the Monte Carlo calculations. To do so, the dose rate constants for media different than water are calculated based on the dose absorbed in an element of water placed in the phantom. For the radial functions, the problem is less relevant as they are relative functions and the energy of the radiation does not vary too much with distance.

The classical water equivalent materials used for high energy dosimetry, like PMMA but even solid water WT1, are not adapted for low energy photons. Their use can induce differences in the radial dose function up to 15% at 6 cm from a ^{103}Pd source and close to 10% for ^{125}I in the case of WT1. The results obtained with RW1 are much closer to those for water however, for both isotopes. This solid water has been specially engineered for low energy photons, so the result was expected. This may not be a real problem however for the determination of dosimetric characteristics of solid water as the normal procedure, recommended recently by AAPM (Rivard et al. 2004), is to complement the measurements with Monte Carlo calculations in order to obtain the dosimetric functions in water, which are the data that are used in the treatment planning systems. The measurements are only used then to check the Monte Carlo calculations and could probably be done in any material under the condition that the composition and density of that material is well known.

The exact composition and density of the materials used in this study become consequently also of importance. It was unfortunately not possible to check the chemical composition of the plastics we have used so this introduces a supplementary uncertainty. One of the solid water plastics, commonly available, that we have used is Solid Water™ RMI-457 which differs from the WT1 proposed by White et al. (1978a) by its density of 1.03 compared to the density of 1.015 tabulated in ICRU44 (1989) for the WT1. We have indeed confirmed this density. However, it does not lead to

significant differences in the calculations. Some authors (Patel et al. 2001) have performed an analysis of RMI-457 and claim that at least for the analysed sample the composition was different from the composition given by the vendor in the quantity of Ca it contained. However, in this study, we have also used two other phantom materials. We have obtained a coherence of the results that would not have been possible if the composition of our sample of Solid Water had been the one proposed by Patel et al.

On the other hand, the comparison of the radial functions calculated in water and in body tissues is perhaps more worrysome as it questions the very fact of using water as a tissue substitute for low energy photons as it is done in the treatment planning systems. This could induce an overestimation of the dose at a few centimetres from the sources, at least in the tissues we have studied. This is only a very preliminary conclusion however, but it shows that, as there can be variations even between soft tissues depending on the content of high-Z elements, it could probably be very interesting to assess the effect of using the real patient geometry for seeds as it is done in external radiotherapy and to take into account the heterogeneities. This is however not a trivial problem as the knowledge of the densities of the tissues, or electron densities, which is the information directly accessible from CT-scan, is not sufficient and one should be able to discriminate between soft tissues of various compositions.